ATTITUDE STABILIZATION OF SPACECRAFT USING MOVING MASSES

by

Juran Hwang

THESIS

Submitted in partial fulfillment of the requirements
for the degree of Master of Science in Aerospace Engineering at
The University of Texas at Arlington

August, 2016

Arlington, Texas

Supervising Committee:

Atilla Dogan, Supervising Professor

Hyejin Moon

Alan P. Bowling

Copyright © by Juran Hwang 2016

All Rights Reserved

To my Dad

ABSTRACT

ATTITUDE STABILIZATION OF SPACECRAFT

USING MOVING MASSES

Juran Hwang, MS

University of Texas at Arlington, 2016

Supervising Professor: Atilla Dogan

This research investigates the ability of stabilizing spacecraft rotational motion by internal mass actuation. The mass actuation mechanism consists of three internal masses placed along the three axes at some offset distance that can move to induce inertial forces and moments and change the inertia matrix and center of mass. A set of nonlinear equations of motion are developed to model the motion, both orbital and rotational dynamics and kinematics, of a spacecraft with mass and inertial variation due to internal mass actuation, under the gravitational field of Earth. The equations inherently include the inertia effect of the mass motion on the orbital and rotational dynamics. Translational kinematics is written in terms of altitude, longitude and latitude, and the rotational kinematics is expressed relative to the local horizontal and local vertical frame. The equations of motion are first used to analyze two nominal flight conditions: (1) spacecraft facing towards Earth on a circular

orbit, and (2) spacecraft spinning around the axis towards Earth on a circular orbit. A NDI (Nonlinear Dynamic Inversion) based controller is designed to stabilize the spacecraft by mass actuation in the first nominal condition from a tumbling condition. This controller is evaluated at three levels in terms of the fidelity of the spacecraft model: (1) only rotational dynamics equations, (2) rotational dynamics coupled with the nominal orbital motion, and (3) the full nonlinear 6-DOF model. The simulation results demonstrate that mass actuation can achieve detumbling of the spacecraft in all three cases with some steady state error when acceleration, speed, and position constrains are imposed on the mass actuators.

ACKNOWLEDGMENT

I would like to express my most sincere appreciation to supervising professor, Dr. Dogan, for his guidance, patience and encouragement not only for the thesis but throughout my master's course as a graduate advisor. Without his guidance and support, I wouldn't have reached my goal.

I would like to thank Republic of Korea army for giving me the opportunity to broaden and deepen my knowledge in the Aerospace Engineering program at UTA.

I thank Dr. Hejin Moon and Dr. Allen Bowling for their roles on my thesis committee. I am inspired so much by their unstoppable passion and hard work for educating. None of this would be possible without these educators.

I am grateful for the love and support of my family and Paul. The completion of this thesis will mean a lot to them. I am fortunate enough to be part of them.

Table of Contents

Abstract **iv**

Acknowledgments **vi**

1 INTRODUCTION **1**

1.1 Background 1

1.2 Research Objective and Thesis Content 2

2 EQUATIONS OF MOTION **4**

2.1 Mathematical concepts 4

2.1.1 Inertial Frame 4

2.1.2 Local Frame 5

2.1.3 Body Frame 6

2.1.4 Vectrix Formalism and Rotation Matrices 6

2.2 Equation of Motion 9

2.2.1 Translational Dynamics 9

2.2.2 Rotational Dynamics 11

2.2.3 Translational Kinematics 12

2.2.4 Rotational Kinematics 13

2.2.5 State-Space Form of the Dynamics Equations 16

3 NOMINAL CONDITION AND OPEN LOOP RESPONSE SIMULATION 18

3.1 Simulation of Nominal Flight 19

3.1.1 Circular Orbit with No Spinning 19

3.1.2 Circular Orbit with Spinning 20

3.2 Open-loop Response to Mass Actuation 21

3.2.1 Rotational Dynamics Only 22

3.2.2 Rotational Dynamics Coupled with Orbital Motion 25

3.2.3 Full 6-DOF Motion 27

4 MASS-ACTUATION-BASED CONTROLLER DESIGN FOR DETUMBLING 29

5 CLOSED-LOOP SIMULATION 34

5.1 Rotational Dynamics Only 34

5.2 Rotational Dynamics Coupled with Orbital Motion 37

5.3 Full 6-DOF Motion 39

6 CONCLUSION 43

Appendix 45

A TRANSFORMATION FROM EARTH-FIXED FRAME TO LOCAL FRAME 46

B NOMINAL CONDITION ANALYSIS 50

List of Figures

2.1 Inertial frame(Earth-Fixed) 5

2.2 Local frame 5

2.3 Spacecraft's body frame 6

2.4 Reference frames and the rotation matrices 9

2.5 Gravitational moments acting on rigid body center of mass and moving mass 11

2.6 Rotation from inertial frame to local frame 16

3.1 Circular orbital motion without spin 20

3.2 Circular orbit with spinning 21

3.4 Response when rotational dynamics only with u=[1,0,0] 23

3.5 Response when rotational dynamics only with u=[0,1,0] 23

3.6 Response when rotational dynamics only with u=[0,0,1] 24

3.7 Inertia matrix when $u = [1, 0, 0]$ w.r.t the initial position of mass actuators 24

3.8 ω_B w.r.t the initial position of mass actuators 25

3.9 Response when rotational dynamics only with u=[1,0,0] 26

3.10 Response when rotational dynamics only with u=[0,1,0] 27

3.11 Response when rotational dynamics only with u=[0,0,1] 27

3.12 Full 6-DOF motion response when $u = [1, 0, 0]$ 28

4.1 NDI+PID feedback control structure 32

5.1 Rotational dynamics response in closed-loop with no acceleration limit 35

5.2 Rotational dynamics response in closed-loop with 1 m/s^2 acceleration limit . 35

5.3 Rotational dynamics response in closed-loop with 1 $/m^2$ limit and position 2 36

5.4 Comparison of ω_B w.r.t acceleration limit 37

5.5 Change in ω_B w.r.t mass and position of the mass actuator 38

5.6 Comparision of $\ddot{\rho}_{mj}$ w.r.t. the coupling of orbital motion 39

5.7 Full simulation with $\omega_{B_0} = [0, 0, 0]deg/s$ 40

5.8 Position of mass actuators 41

5.9 Full simulation with $\omega_{B_0} = [1, -1, 0.8]deg/s$ 42

A.1 Depiction of Earth-fixed and local frame 48

CHAPTER 1

INTRODUCTION

1.1 Background

Spacecraft attitude determination and control (ADC) plays a crucial role in the accomplishment of mission of the spacecraft. As of today, many spacecraft have been successfully launched and most have performed well as they were designed. Unfortunately, some of them failed their missions. For example, on April 3, 1973, Salyut 2 was in uncontrolled state from tumbling caused by an explosion or a wildly firing thruster [1]. Recently, there was another accident happened on March 26, 2016, Japan's Hitomi was tumbling in space induced by a malfunction [2]. Spacecraft may be in unstable state by many factors such as the solar radiation, flexible part of the spacecraft, or internal motion in manned spacecraft. The spacecraft should be stabilized by its ADC system. As long as the spacecraft is in the stable state, it can fulfill its own function and carry out the mission during its whole lifespan. In other words, if the spacecraft is tumbling, it would not be possible to acquire the desired attitude to point toward the Earth and determine the spacecraft's trajectory. For this reason, ADC in the spacecraft is closely related to the spacecraft's performance and have been studied and developed so for.

There are two types of commonly used stabilization devices. The passive type uses spin stabilization or gravity gradient. This passive controller is simple to install but easy to be disturbed by external torque (e.g., gravity gradient, aerodynamic drag, and solar radiation). The second and commonly used type of stabilization devices include reaction wheels, control moment gyros (CMG), magnetic torque and thrusters. These actuators are able to provide more accurate orientation and high agility of the response but need to accept high expense [1].

Mass actuation is another active stabilization method proposed for various applications such as spacecraft [7-12], airplane [3,4] and warhead [5]. Ref. [6–9] dealt with two internal moving masses for attitude stabilization. Particularly, for micro satellites in Ref. [8] and [7], instead of installing heavy actuators, the spacecraft may take an advantage of utilizing its movable mass for detumbling. Also, Ref. [10] presents the optimal recofiguration of movable fuel tank to control the spacecraft's attitude. In Ref. [11], two masses moving along x-axis are used for detumbling an asymmetric space station.

1.2 Research Objective and Thesis Content

This thesis investigates the feasibility of mass actuation in detumbling a spacecraft flying on a circular orbit in the gravitational field of Earth. In Section 2, it develops the equations of motion and computer simulation that model the dynamic effect of internal mass motion on the rotational and orbital motion of the spacecraft. The orbital motion kinematics is represented in terms of altitude, longitude and latitude. The rotational kinematics is written in terms of 3-2-1 Euler angles relative to the local horizontal and local vertical frame. Two different nominal flight conditions on circular orbit are simulated in Section 3 : (1) spacecraft pointing towards Earth, and (2) spacecraft spinning around the axis towards

Earth. In this section, open-loop responses of the spacecraft to various mass actuation are analyzed in both nominal conditions. Section 4 gives the details of the control design, using a nonlinear dynamic inversion method to stabilize the spacecraft from a tumbling state. In Section 5, the detumbling controller is evaluated in closed loop using spacecraft models with increasing fidelity: (1) rotational dynamics only, (2) rotational dynamics coupled with the nominal orbital motion, and (3) the full 6-DOF model. Conclusions and future work are discussed in Section 6.

CHAPTER 2

EQUATIONS OF MOTION

This chapter presents the mathematical concepts for spacecraft dynamics modelling and the equations of motion for spacecraft with moving masses. A set of nonlinear, 6-DOF, equations of motion from Ref. [12] is modified for spacecraft. For spacecraft orbital motion, translational kinematics is written in the local frame.

2.1 Mathematical concepts

2.1.1 Inertial Frame

The inertial frame is fixed to the Earth, thus it rotates at the same speed as the Earth's rotation. In this system, the origin is at the center of Earth and z-axis, z_E, points towards the North pole and x_E-axis is towards the point on the surface coinciding the latitude of 0 deg (Equator) and the longitude of 0 deg (Greenwich). Y_E-axis is normal to x_E-z_E plane to complete the right handed Cartesian coordinate system.

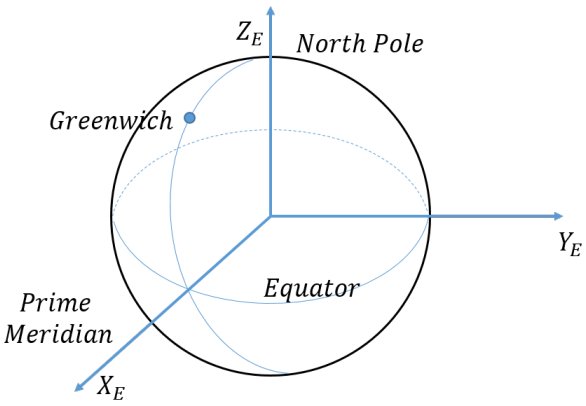

Figure 2.1: Inertial frame(Earth-Fixed)

2.1.2 Local Frame

The spacecraft position is tracked in terms of altitude, latitude, and longitude. In order to express and simulate its trajectories, it is necessary to transform this geodetic coordinate to a local rectangular coordinate system. The local frame denoted with the letter L. The x_L of the local frame always points at the spacecraft from the origin of Earth. z_L-axis is parallel to the direction of spacecraft velocity and perpendicular to x_L-axis. y_L-axis is normal to x_L-z_L plane to complete the right handed Cartesian coordinate system.

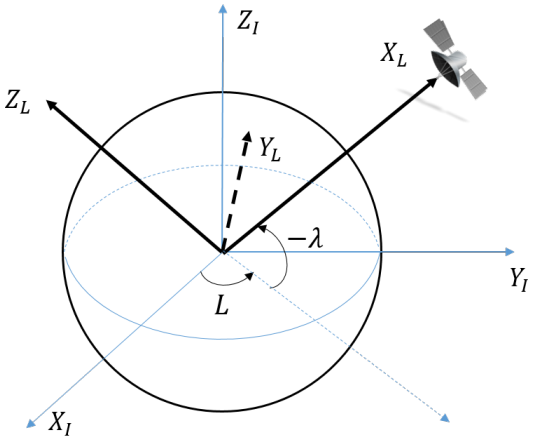

Figure 2.2: Local frame

The rotation from the inertial frame to the local frame can be achieved by a rotation by angle L around z_E-axis, and then the second rotation by angle $-\lambda$ around y_E-axis depicted in Fig. 2.2 and a more detailed discussion in appendix A.

2.1.3 Body Frame

Spacecraft translational and rotational dynamics are described in this thesis using body frame representation. The body frame denoted with the letter B is the frame translates and rotates with the spacecraft. In this study, the center of mass of the entire spacecraft system moves as the internal masses move. Thus, the origin of the body frame is not placed at the center of mass of the whole spacecraft system. Instead, the body frame origin is placed at the center of mass of the rigid body part of the spacecraft, i.e., the spacecraft system excluding the moving masses.

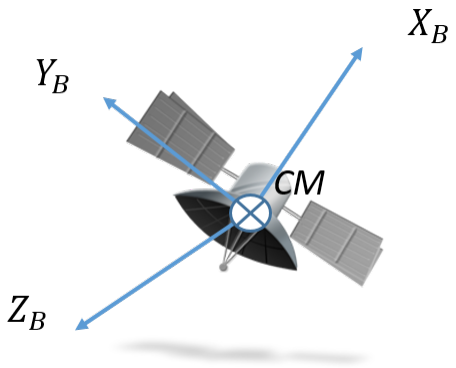

Figure 2.3: Spacecraft's body frame

2.1.4 Vectrix Formalism and Rotation Matrices

The equations of motion of spacecraft in this thesis are written in the matrix form. This is because the matrix equations are more proper for carrying out simulations in MATLAB. To write a vector in matrix form, vectrix formalism is adapted from Ref. [12]. The matrix

form of the equations make use of vector representations in a specified frame instead of vectors. For example, the vectrix of X frame is defined to be the array of the unit vectors of its axes and is denoted by

$$[\hat{\underline{X}}] = \begin{bmatrix} \hat{\underline{i}}_X \\ \hat{\underline{j}}_X \\ \hat{\underline{k}}_X \end{bmatrix} \tag{2.1}$$

Hence, vector $\underline{a}$ can be written as

$$\underline{a} = [\hat{\underline{X}}]^T a \tag{2.2}$$

where a is the representation of vector $\underline{a}$ in X frame and a 3x1 matrix. There are several reference frames so the representation of vectors in multiple frames are used in the matrix form. Note that the relationship between the vectrices of the two frames are defined by the rotation matrix between the two frames,

$$[\hat{\underline{X}}] = \mathbf{R}_{XY}[\hat{\underline{Y}}] \tag{2.3}$$

where $\mathbf{R}_{XY}$ is the rotation matrix from the X frame to the Y frame. Representations or components of a vector in different frames are also related through the same rotation matrix. For example, representation of vector $\underline{a}$ in X frame can be written in terms of its representation in Y frame as

$$a_X = \mathbf{R}_{XY} a_Y \tag{2.4}$$

Due to the orthogonal property of rotation matrices, the inverse rotation from Y to X is performed by using the transpose of $\mathbf{R}_{XY}$.

$$a_Y = \mathbf{R}_{XY}^T a_X \tag{2.5}$$

The equations of motion for the spacecraft written in matrix form are used to facilitate numerical simulations. The matrix equations include the rotation matrices to transform the components of a vector from one frame to another. Typically, a vector is written in the most convenient frame (e.g., gravity vector, altitude, latitude, and longitude written in the local frame) and then transformed to the frame of interest for simulation or dynamical analysis (e.g., the inertial frame or spacecraft body frame). The rotation matrices are defined between the reference frames in this thesis are shown in figure 2.4. In this study, there are two rotation matrices used, $\mathbf{R_{BL}}$ and $\mathbf{R_{LI}}$. $\mathbf{R_{BL}}$ is rotation matrix from local frame to body frame as

$$\mathbf{R_{BL}} = \begin{bmatrix} cos\psi cos\theta & cos\theta sin\psi & -sin\theta \\ -cos\phi sin\psi + sin\phi sin\theta cos\psi & cos\phi cos\psi + sin\phi sin\theta sin\psi & sin\phi cos\theta \\ sin\theta sin\psi + cos\phi sin\theta cos\psi & -sin\phi cos\psi + cos\phi sin\theta sin\psi & cos\phi cos\theta \end{bmatrix} \tag{2.6}$$

$\mathbf{R_{LI}}$ is rotation matrix from inertia frame to local frame as

$$\mathbf{R_{LI}} = \begin{bmatrix} cos\lambda cosL & cos\lambda SinL & sin\lambda \\ -sinL & cosL & 0 \\ -sin\lambda cosL & -sin\lambda sinL & cos\lambda \end{bmatrix} \tag{2.7}$$

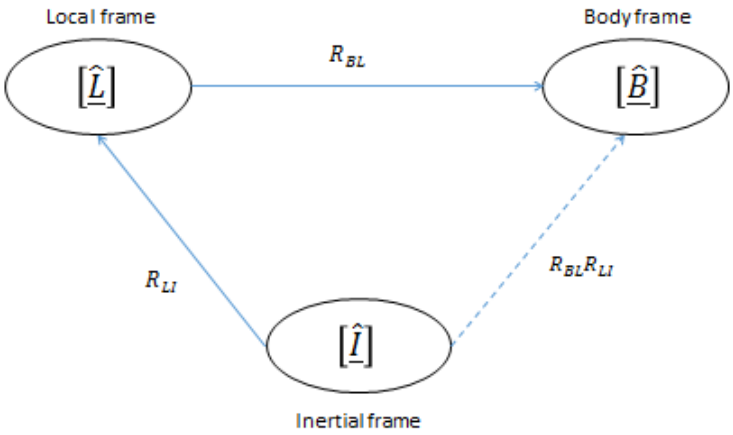

Figure 2.4: Reference frames and the rotation matrices

2.2 Equation of Motion

2.2.1 Translational Dynamics

Translational dynamics equation of the spacecraft in matrix form is

$$\begin{aligned}\dot{V_B} = \frac{1}{m_t}F_B - \mathbf{S}(\rho_{cm,t})\dot{\omega}_B + \mathbf{S}(\omega_B)V_B - \mathbf{S}^2(\omega_B)\rho_{cm,t} \\ +2\mathbf{S}(\omega_B)\frac{1}{m_t}\sum_{j=1}^{k} m_j\dot{\rho}_{mj} - \frac{1}{m_t}\sum_{j=1}^{k} m_j\ddot{\rho}_{mj}\end{aligned} \tag{2.8}$$

where V_B is the representation of the velocity of the spacecraft, $V_B = [u\, v\, w]^T$ and F_B is the external forces acting on the spacecraft expressed in the body frame. $\rho_{cm,t}$ is the position of the center of the mass of total system. ω_B is the representation of the angular velocity vector of the spacecraft, $\omega_B = [p\, q\, r\,]^T$. m_t is the total mass of the system. m_j is the mass of j^{th} mass actuator, $j = 1, 2, 3$. ρ_{mj} is the position of the j^{th} mass actuator from the initial position which is the center of mass of spacecraft. All terms in the equation are expressed in the body frame with respect to inertial frame. Also, note that $\mathbf{S}(\cdot)$ is the skew-symmetric matrix operation on the representation of a vector and defined as

$$\mathbf{S}(x) = \begin{bmatrix} 0 & c & -b \\ -c & 0 & a \\ b & -a & 0 \end{bmatrix} \tag{2.9}$$

for an arbitrary vector $\underline{x}$ with the representation $[a\, b\, c\,]^T$.

The external force, F_B, is expressed as

$$F_B = F_a + F_g \tag{2.10}$$

where $F_a = [F_x,\, F_y,\, F_z]^T$ is in the body frame of the applied force due to external sources other than gravity such as thruster. F_a depends on nominal condition analyzed in appendix B. F_g is the gravitational force using the law of gravitational attraction as

$$F_g = [L]^T \begin{bmatrix} -\left(M + \sum_{j=1}^{k} m_j\right) \dfrac{\mu}{(R+h)^2} \\ 0 \\ 0 \end{bmatrix} = [B]^T \mathbf{R_{BL}} \begin{bmatrix} -\left(M + \sum_{j=1}^{k} m_j\right) \dfrac{\mu}{(R+h)^2} \\ 0 \\ 0 \end{bmatrix} \tag{2.11}$$

where $[L]^T = [B]^T \mathbf{R_{BL}}$ which is the relationship between local frame and body frame using rotation matrix, M is the mass of rigid body of spacecraft and m_j is the mass of j^{th} moving mass actuator, μ is the standard gravitational parameter, $3.989 \times 10^{14}\, m/s^2$.

Fig. 2.5 depicts the gravitational force vectors acting on rigid body center of mass, $\underline{f}_M$, and on the j^{th} mass, $\underline{f}_{m_j}$. Note that these two vectors are not along the same direction since each vector points towards the center of Earth from different positions. However, the formulation in Eq. (2.11) assumes them to be pointing in the same direction, which can be justified due to the fact that the distance between these two points is much smaller than

the distances from the center of Earth.

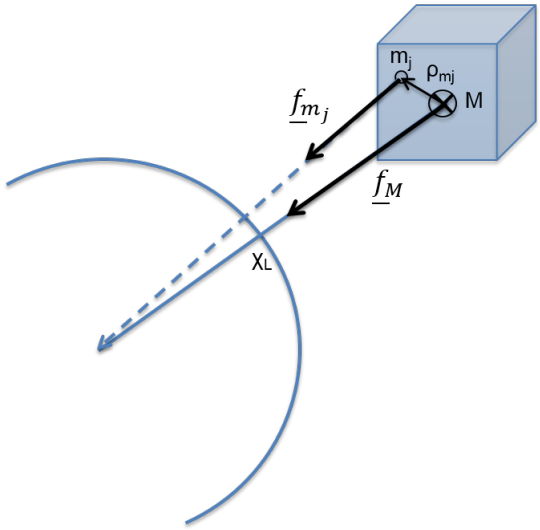

Figure 2.5: Gravitational moments acting on rigid body center of mass and moving mass

2.2.2 Rotational Dynamics

The matrix form of the rotational dynamics is

$$\begin{aligned}\dot{\omega}_B = \underline{\underline{\mathbf{I}}}_{\mathbf{t}}^{-1}\{M_B + \left[\mathbf{S}(\omega_B)\underline{\underline{\mathbf{I}}}_{\mathbf{t}} - \underline{\underline{\dot{\mathbf{I}}}}_{\mathbf{m}}\right]\omega_B + m_t\mathbf{S}(\rho_{cm,t})\dot{V}_B \\ -m_t\mathbf{S}(\rho_{cm,t})\mathbf{S}(\omega_B)\mathbf{S}(\omega_B)V_B + \sum_{j=1}^{k} m_j\mathbf{S}(\rho_{mj})\ddot{\rho}_{mj}\}\end{aligned} \tag{2.12}$$

where $\underline{\underline{\mathbf{I}}}_{\mathbf{t}}$ is the inertia matrix of spacecraft including the moving masses, $\underline{\underline{\dot{\mathbf{I}}}}_{\mathbf{m}}$ is the time rate of change in the inertia matrix of the moving masses, M_B is the moment of the external forces around the origin of the spacecraft body frame and expressed in body frame as

$$M_B = M_a + M_g \tag{2.13}$$

where M_a is applied force from control momentum gyros or momentum wheel or other

actuators installed in spacecraft. M_g is gravitational moment due to the rigid body mass, and the moving masses, around the origin of the body frame. Therefore,

$$M_g = -\left[M\mathbf{S}(\rho_{cm}) + \sum_{j=1}^{k} m_j \mathbf{S}(\rho_{mj})\right] \mathbf{R_{BL}} \begin{bmatrix} -\dfrac{\mu}{(R+h)^2} \\ 0 \\ 0 \end{bmatrix} \tag{2.14}$$

2.2.3 Translational Kinematics

The translational kinematics is the formulation for the time rate of change of the position vector in terms of the translational velocity vector. Position vector $\underline{r}_B$ relative to the center of Earth is most conveniently expressed in the local frame as

$$\underline{r}_B = [L]^T \begin{bmatrix} R+h \\ 0 \\ 0 \end{bmatrix} \tag{2.15}$$

where R is the Earth mean radius, 6,367,435 m and h is altitude measured from Earth's surface. Since $[L] = \mathbf{R_{LI}}[I]$, $\underline{r}_B$ can be expressed in the inertial frame and differentiated as

$$\begin{aligned} \dot{\underline{r}}_B = [I]^T \frac{d}{dt} \left\{ \mathbf{R}_{\mathbf{LI}}^T \begin{bmatrix} R+h \\ 0 \\ 0 \end{bmatrix} \right\} = \\ [I]^T \begin{bmatrix} cos\lambda cosL & -(R+h)sin\lambda cosL & -(R+h)cos\lambda sinL \\ cos\lambda sinL & -(R+h)sin\lambda sinL & (R+h)cos\lambda cosL \\ sin\lambda & (R+h)cos\lambda & 0 \end{bmatrix} \begin{bmatrix} \dot{h} \\ \dot{\lambda} \\ \dot{L} \end{bmatrix} \end{aligned} \tag{2.16}$$

In order to track the spacecraft in terms of altitude (h), latitude (λ), and longitude(L), let $\chi = [h\ \lambda\ L]^T, \dot{\chi} = [\dot{h}\ \dot{\lambda}\ \dot{L}]^T$and $\boldsymbol{\epsilon}$ as

$$\boldsymbol{\epsilon} = \begin{bmatrix} cos\lambda cosL & (R+h)sin\lambda cosL & -(R+h)cos\lambda sinL \\ cos\lambda sinL & -(R+h)sin\lambda sinL & (R+h)cos\lambda cosL \\ sin\lambda & (R+h)cos\lambda & 0 \end{bmatrix} \tag{2.17}$$

Therefore, translational kinematics can be expressed in inertial frame, $\underline{\dot{r}}_B = [I]^T \boldsymbol{\epsilon} \dot{\chi}$ and $\underline{\dot{r}}_B = [B]^T V_B$ in body frame. Note that $[I] = R_{LI}^T R_{BL}^T [B]$. Thus, $\underline{\dot{r}}_B$ is rewritten from the above two equations as

$$\underline{\dot{r}}_B = [B]^T \mathbf{R_{BL}} \mathbf{R_{LI}} \boldsymbol{\epsilon} \dot{\chi} = [B]^T V_B \tag{2.18}$$

Canceling out the common vectrix $[B]^T$, translational kinematics equation is now written in terms of (h, λ, L)

$$\dot{\chi} = \boldsymbol{\epsilon}^{-1} \mathbf{R_{LI}^T} \mathbf{R_{BL}^T} V_B \tag{2.19}$$

2.2.4 Rotational Kinematics

The rotational kinematics equation in matrix form is from Poisson's equation

$$\dot{\mathbf{R}}_{\mathbf{BL}} = \mathbf{S}(\omega_{_{BL}}) \mathbf{R_{BL}} \tag{2.20}$$

where $\omega_{_{BL}}$ is the representation of the angular velocity vector of the spacecraft with respect to local frame expressed in its own body frame as $\omega_{_{BL}} = [\omega_x\ \omega_y\ \omega_z]^T$.

The rotational motion of the spacecraft is written in terms of Euler angles as

$$\begin{bmatrix} \dot{\phi} \\ \dot{\theta} \\ \dot{\psi} \end{bmatrix} = \begin{bmatrix} 1 & tan\theta sin\phi & tan\theta cos\phi \\ 0 & cos\phi & -sin\phi \\ 0 & sec\theta sin\phi & sec\theta cos\phi \end{bmatrix} \begin{bmatrix} \omega_x \\ \omega_y \\ \omega_z \end{bmatrix} \tag{2.21}$$

There are three angular velocity vectors involved in the equations of motion. Angular velocity of the spacecraft relative to the inertial frame, computed by the rotational dynamics in Eq. (2.12), is $\underline{w}_B$, expressed in the body frame with representation w_B. Angular velocity of the spacecraft relative to the local frame, introduced in the rotational kinematics formulation in Eq. (2.21) is $\underline{w}_{BL}$, expressed in the body frame with representation w_{BL}. The relation of these two rotation matrices should be formulated. This is done by introducing $\underline{w}_L$, the angular velocity vector of the local frame relative to the inertial frame, with its representation in the local frame as w_L. The angular velocity with respect to the inertial frame can be expressed as the sum of the angular velocity with respect to the local frame and the angular velocity of the local frame with respect to the inertial frame, which is formulated as

$$\underline{\omega}_B = \underline{\omega}_{BL} + \underline{\omega}_L \tag{2.22}$$

Using the representations of these vectors as introduced above, this equation can be written in terms of the representations as

$$\omega_B = \omega_{BL} + \mathbf{R_{BL}}\omega_L \tag{2.23}$$

Since the local frame is defined such that x-axis always points towards the spacecraft traveling along the orbit, its angular velocity $\underline{w}_L$ is dependent on the orbital motion. As depicted in Fig. 2.6, rotation from the inertial frame to the local frame can be achieved

by (1) rotating around z-axis by angle L, followed by rotation around y-axis by angle $-\lambda$. Similarly, the angular velocity of the local frame can be written in terms of the angular velocities of these elementary rotations as

$$\underline{\omega}_L = [1]^T \begin{bmatrix} 0 \\ 0 \\ \dot{L} \end{bmatrix} + [L]^T \begin{bmatrix} 0 \\ -\dot{\lambda} \\ 0 \end{bmatrix} = [L]^T \left\{ R_2 \begin{bmatrix} 0 \\ 0 \\ \dot{L} \end{bmatrix} + \begin{bmatrix} 0 \\ -\dot{\lambda} \\ 0 \end{bmatrix} \right\} \tag{2.24}$$

where

$$R_2(-\lambda) = \begin{bmatrix} cos\lambda & 0 & sin\lambda \\ 0 & 1 & 0 \\ -sin\lambda & 0 & cos\lambda \end{bmatrix} \tag{2.25}$$

Carrying out the matrix multiplications in Eq. (2.24) and noting that w_L is the representation in the local frame lead to

$$\omega_L = \begin{bmatrix} sin\lambda\dot{L} \\ -\dot{\lambda} \\ cos\lambda\dot{L} \end{bmatrix} = \begin{bmatrix} 0 & 0 & sin\lambda \\ 0 & -1 & 0 \\ 0 & 0 & cos\lambda \end{bmatrix} \begin{bmatrix} \dot{h} \\ \dot{\lambda} \\ \dot{L} \end{bmatrix} = \epsilon_2 \dot{\chi} \tag{2.26}$$

where

$$\epsilon_2 = \begin{bmatrix} 0 & 0 & sin\lambda \\ 0 & -1 & 0 \\ 0 & 0 & cos\lambda \end{bmatrix} \tag{2.27}$$

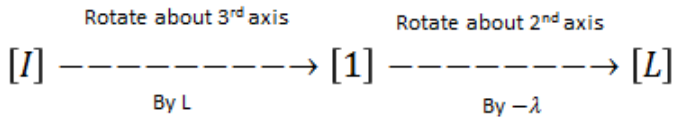

Figure 2.6: Rotation from inertial frame to local frame

2.2.5 State-Space Form of the Dynamics Equations

The dynamics equations written in a compact form as,

$$\dot{V}_B = f_1 \dot{\omega}_{B_R} + c_1 \tag{2.28}$$

$$\dot{\omega}_{B_R} = f_2 \dot{V}_B + c_2 \tag{2.29}$$

where

$$f_1 = -\mathbf{S}(\rho_{cm,t}) \tag{2.30}$$

$$c_1 = \frac{1}{m_t} F_{B_R} \mathbf{S}(\omega_{B_R}) V_B = \mathbf{S}^2(\omega_{B_R}) \frac{1}{m_t} \sum_{j=1}^{k} m_j \dot{\rho}_{mj} - \frac{1}{m_t} \sum_{j=1}^{k} m_j \ddot{\rho}_{mj} \tag{2.31}$$

$$f_2 = m_t \underline{\underline{\mathbf{I}}}_{\mathbf{t}}^{-1} \mathbf{S}(\rho_{cm,t}) \tag{2.32}$$

$$c_2 = \underline{\underline{\mathbf{I}}}_{\mathbf{t}}^{-1} \left\{ M_{B_R} + \left[\mathbf{S}(\omega_{B_R}) \underline{\underline{\mathbf{I}}}_{\mathbf{t}} - \dot{\underline{\underline{\mathbf{I}}}}_{\mathbf{m}} \right] \omega_{B_R} - m_t \mathbf{S}(\rho_{cm,t}) \mathbf{S}(\omega_{B_R}) \mathbf{S}(\omega_{B_R}) V_B \sum_{j=1}^{k} m_j \mathbf{S}(\rho_{mj}) \ddot{\rho}_{mj} \right\} \tag{2.33}$$

Note that the above set of equations, Eq.(2.28) and Eq.(2.29), are not in the standard state-space form, which is the most convenient for numerical simulation. After some manipulation, these equations are rewritten as

$$\dot{V}_B = (\mathbf{I_{3\times 3}} - f_1 f_2)^{-1} (f_1 c_2 + c_1) \tag{2.34}$$

$$\dot{\omega}_{B_R} = (\mathbf{I_{3\times 3}} - f_2 f_1)^{-1}(f_2 c_1 + c_2) \tag{2.35}$$

Eqs. (2.32) and (2.33) are the dynamics equations written in the state-space form and to be used in linearization of equations of motion and computer simulations.

CHAPTER 3

NOMINAL CONDITION AND OPEN LOOP RESPONSE SIMULATION

The equations of motions are implemented in a Matlab/Simulation environment to evaluate controller performance in detumbling tasks. This chapter presents the simulations of nominal condition flights and response of the spacecraft to mass actuation. As stated before, three internal masses are considered, each of which moves along one of the three axes. For the purpose of control design, the commanded accelerations of the internal masses are defined as the control input variables. The saturation limits of the mass motion in acceleration, speed and position are included in the simulation model. The motion dynamics of each mass actuator, considering all the saturation limits, model the relations between the acceleration, speed, and position, e.g., the speed and acceleration go to zero at the time when the position reaches its limit, while the commanded acceleration is still nonzero. In the discussions below, the masses that move along x-axis, y-axis, and z-axis are referred to as ma_1, ma_2, and ma_3, respectively. This means the control input variables are

$$u = [\ddot{\rho}_{m_{1_x}}\ \ddot{\rho}_{m_{2_y}}\ \ddot{\rho}_{m_{3_z}}]^T \tag{3.1}$$

Although no particular spacecraft is represented in the simulation, the following mass and inertia parameters are used in the simulations. The mass of the rigid part of the spacecraft is 400 kg and the body frame of the spacecraft is assumed to be the principal axes, i.e., the inertia matrix is diagonal with $I_{xx} = 900$, $I_{yy} = 200$, and $I_{xx} = 130$ $kg.m^2$. The total mass of the spacecraft and the inertia matrix will be different depending on the amount and position of the mass actuators.

3.1 Simulation of Nominal Flight

In the simulation environment discussed above, the nominal flight conditions defined and analyzed in Appendix B are simulated. This is to validate the accuracy of the simulation in the nominal conditions before any other open loop or closed loop simulations are carried out. Since the nominal conditions are defined to have no internal mass motion, the input variables (i.e., the acceleration commands of the three masses) are set to zero. The simulation of nominal flight was divided into two specific cases ; non-spinning and spinning along x_B-axis. In both cases, the fixed positions of the three masses are set such that the center of mass of the spacecraft is at the origin of the body frame. The dynamic simulation is started with the initial conditions of the state variables at their nominal values. It is expected that all the variables should stay at their nominal values.

3.1.1 Circular Orbit with No Spinning

In this section, the nominal condition is when the spacecraft travels in a circular orbit without spinning, but always facing Earth. Simulation results are presented in Fig. 3.1. From the nominal condition analysis, the nominal values of state variables are given that translational velocity of spacecraft, $V_{B_0} = [0,\ 0,\ 7998]^T\ km/s$ and rotational velocity, $\omega_{B_0} =$

[0, -0.007, 0] ^{T} deg/s. The altitude, h_0 and latitude, L_0 are specified and should be constant at 200 km and 0 deg respectively. Also, the time rate of change of latitude is $\dot{\lambda}_0 = 0.07$ deg/s so, λ is linearly increasing as the spacecraft is orbiting the Earth.

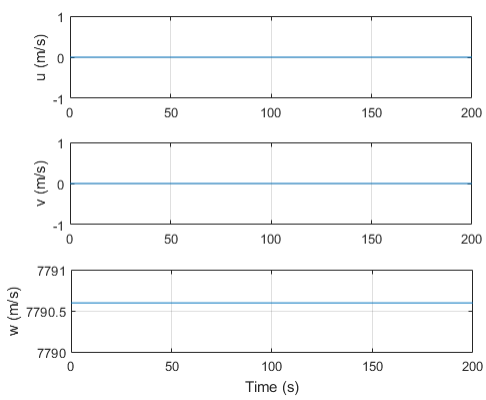

(a) Translational velocity

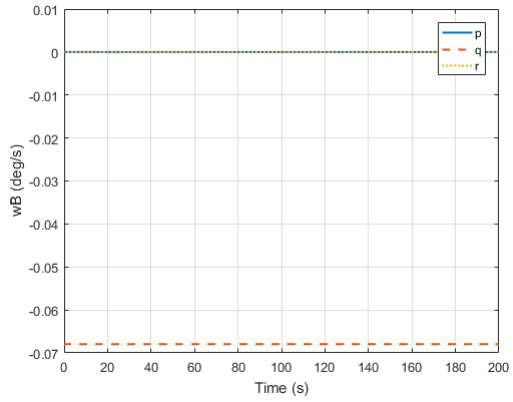

(b) Rotational velocity

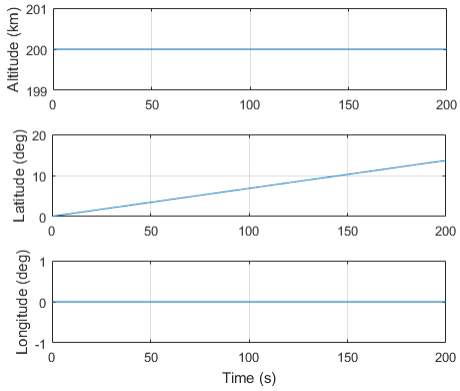

(c) Translation Kinematics

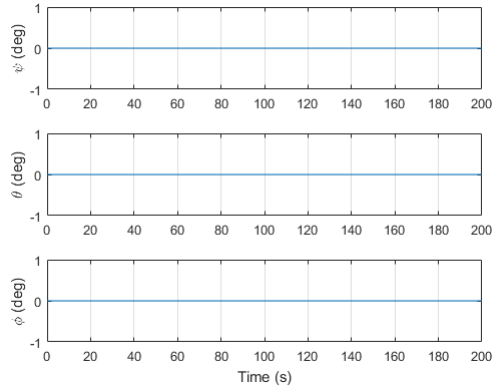

(d) Eulear angles

Figure 3.1: Circular orbital motion without spin

3.1.2 Circular Orbit with Spinning

As shown in Fig. 3.2, the spacecraft was in orbital motion with a simple spin along x_B-axis, which is always aligned with x_L-axis. The p_0 is specified as 1 deg/s. u is zero and v, w, q, and r are some trigonometric functions of time. The altitude and longitude are

constant in this nominal flight.

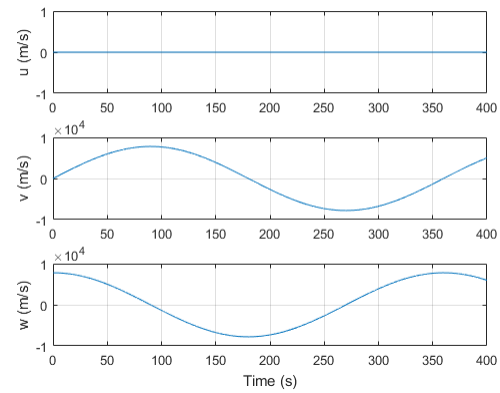

(a) Translational velocity

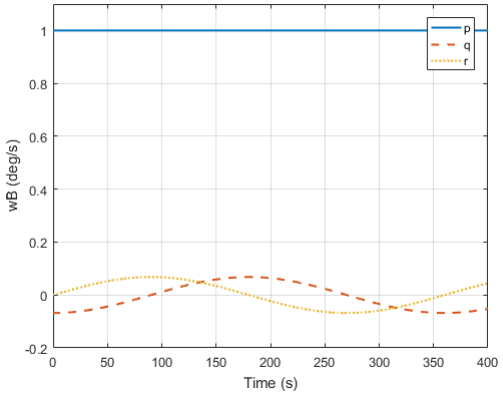

(b) Rotational velocity

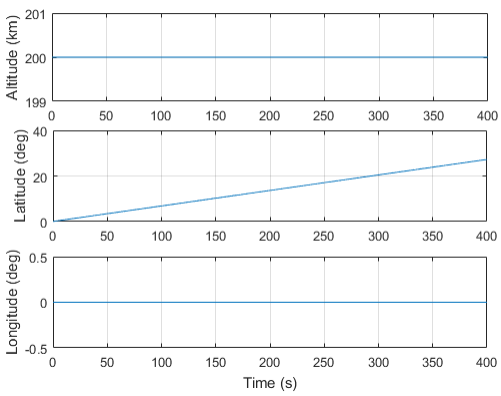

(c) Translation Kinematics

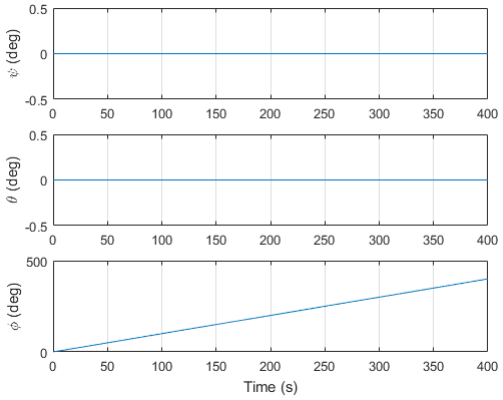

(d) Euler Angles

Figure 3.2: Circular orbit with spinning

3.2 Open-loop Response to Mass Actuation

Since the open-loop system was validated in nominal condition, it can now show the proper rotational dynamics response induced by the mass actuation. The open-loop response to mass actuation was simulated and examined in phases as follows.

(1) Simulation of mass actuation with rotational dynamics.

(2) Simulation of mass actuation with rotational dynamics coupled with the nominal orbital motion.

(3) Simulation of mass actuation with full 6-DOF equations.

The simulations were conducted with different control inputs, i.e., different acceleration of mass actuators as u = [1, 0, 0], [0, 1, 0], [0, 0, 1]. The mass accelerations start at 5 s. It means the one mass actuator moves with 1 m/s^2 of acceleration at each time until speed and/or position limits are reached. The position limit was ± 2 m and speed limit was ± 10 m/s.

3.2.1 Rotational Dynamics Only

In this section, only the response of rotational dynamics was examined. In other word, the spacecraft was stationary and was not in orbital motion. As a result, there was no translational coupling and external force exerted on the spacecraft. For simulation, only the equation of rotation dynamics was used in the system. From Eq. (2.12), the general form of rotational dynamics, after canceling out the translational term, rotational dynamics is reduced to

$$\dot{\omega}_B = \underline{\underline{\mathbf{I}}}_{\mathbf{t}}^{-1}\{M_B + \left[\mathbf{S}(\omega_B)\underline{\underline{\mathbf{I}}}_{\mathbf{t}} - \underline{\underline{\dot{\mathbf{I}}}}_{\mathbf{m}}\right]\omega_B + \sum_{j=1}^{k} m_j \mathbf{S}(\rho_{mj})\ddot{\rho}_{mj}\} \tag{3.2}$$

Fig. 3.4 to 3.6 show the change in the rotational velocity with respect to inputs. The initial position of mass actuators were ρ_{m1} = [0, -0.1, 0.1] m, ρ_{m2} = [0.1, 0, 0.1] m and $\rho m3$ = [0.1, 0.1, 0] m. The initial ω_{B_0} was $[0, 0, 0]\, deg/s$. As seen in Fig. 3.4 (a), the mass actuators reached the position limit at 7 seconds after starting to move at 5 seconds while ma_2 and ma_3 were fixed at the initial position. Fig. 3.4 (b) shows that the movement of ma_1 induced the change in q and r mostly. In Fig. 3.5, the movement of ma_2 toward its

limits changed the p and r the most. For ma_3 in Fig. 3.6, also presents that the movement of ma_3 induced the change in p and q mostly.

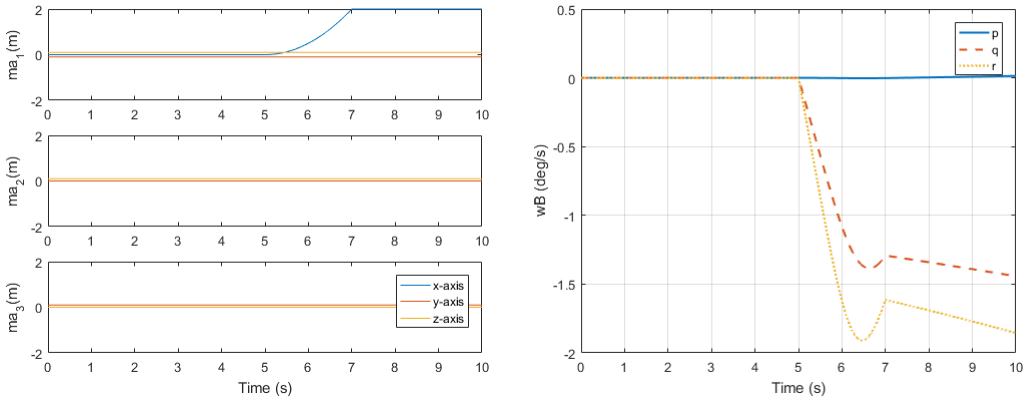

(a) Position of mass actuator (b) ω_B

Figure 3.4: Response when rotational dynamics only with u=[1,0,0]

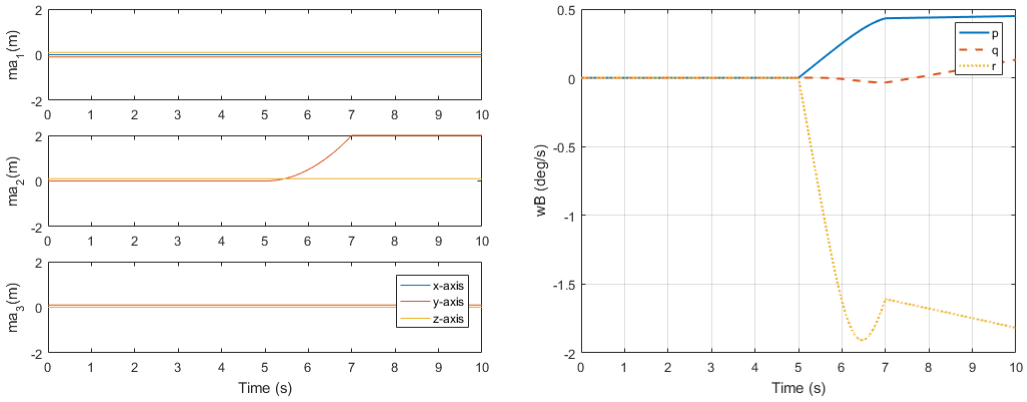

(a) Position of mass actuator (b) ω_B

Figure 3.5: Response when rotational dynamics only with u=[0,1,0]

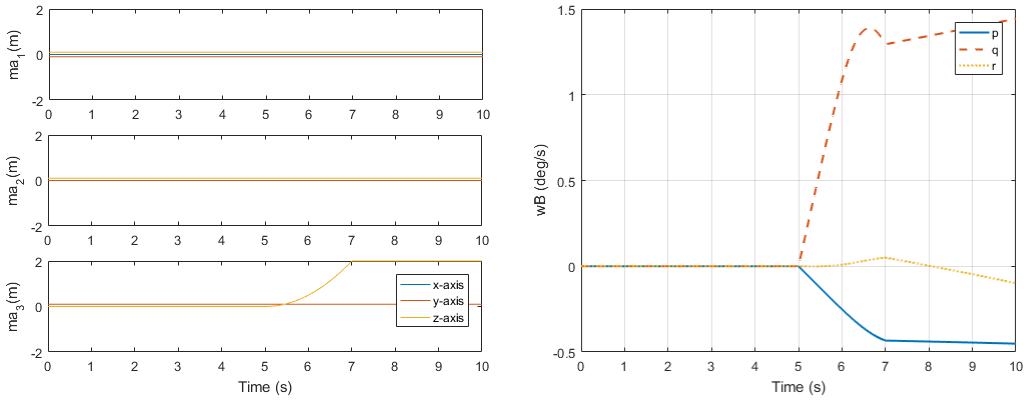

(a) Position of mass actuator (b) ω_B

Figure 3.6: Response when rotational dynamics only with u=[0,0,1]

It is obvious that the internal mass motion caused changes in the inertia matrix. Since the actuators moved parallel to its own axis, the principal axes of inertia have larger change compared to off-diagonal terms.

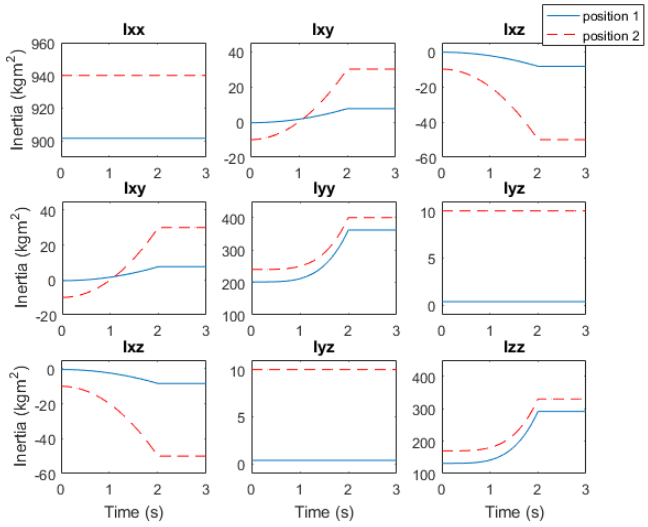

Figure 3.7: Inertia matrix when $u = [1,\ 0,\ 0]$ w.r.t the initial position of mass actuators

In Fig.3.7, when ma_1 moved, the linear motion of ma_1 produced the moment arm which caused the increase in I_{yy} and I_{zz} significantly then others in the inertia matrix. In the

rotational dynamics, Eq. (3.2), it has a product of inertia and rotational velocity. Thus, this may explain why q and r changed considerably.

Furthermore, the inertia matrix was also affected by the position of mass actuators. Since the actuators were placed along the three axes at some offset distance, the effect of this offset was investigated in Fig. 3.8. The position 1 is the position of mass actuators, ma_1 = [0, -0.1, 0.1] m, ma_2 = [0.1, 0, 0.1] m and ma_3 = [0.1, 0.1, 0] m and the position 2 is the position of ma_1 = [0, -0.5, 0.5] m, ma_2 = [0.5, 0, 0.5] m and ma_3 = [0.5, 0.5, 0] m. The inputs were the same as u = [1, 0, 0] for both simulation. Fig. 3.8 indicates that the offset from its axis increases the moment arm, which induce larger change in rotational velocity.

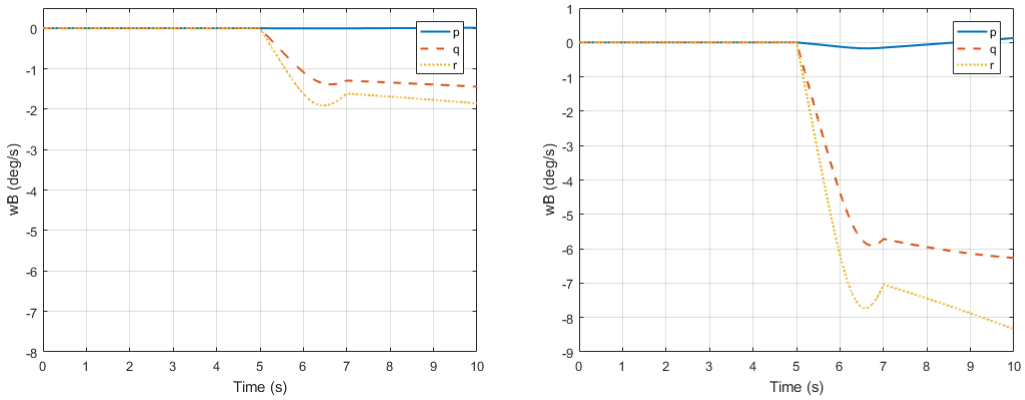

(a) ω_B when position 1 with u = [1, 0, 0] (b) ω_B when position 2 with u = [1, 0, 0]

Figure 3.8: ω_B w.r.t the initial position of mass actuators

3.2.2 Rotational Dynamics Coupled with Orbital Motion

In this section, the spacecraft travels in a circular orbit with constant translational velocity. The rotational dynamics including translational terms are derived in Section 2.2.2.

The general form of rotational dynamics, Eq. (2.12) is used and stated again below,

$$\begin{aligned}\dot{\omega}_B = \underline{\underline{\mathbf{I}}}_{\mathbf{t}}^{-1}\{M_B + \left[\mathbf{S}(\omega_B)\underline{\underline{\mathbf{I}}}_{\mathbf{t}} - \dot{\underline{\underline{\mathbf{I}}}}_{\mathbf{m}}\right]\omega_B + m_t\mathbf{S}(\rho_{cm,t})\dot{V}_B \\ -m_t\mathbf{S}(\rho_{cm,t})\mathbf{S}(\omega_B)\mathbf{S}(\omega_B)V_B + \sum_{j=1}^{k} m_j\mathbf{S}(\rho_{mj})\ddot{\rho}_{mj}\}\end{aligned} \tag{3.3}$$

The initial ω_B = [0, -0.07, 0] m/s. The Fig. 3.9 shows that only r is excited by ma_1 starting to move at 5 seconds from nominal condition. As can be seen in Fig 3.10, when ma_2 moves, both p and r are excited although the change in r is much larger. Also note that when ma_2 reaches its position limit and stops, p goes back to zero while r decreases close to zero, but not exactly. As shown in Fig 3.11, when ma_3 moves, it mainly excites r component. When the rotational motion is coupled with nominal orbital motion, r changed more than other components. This is because, in orbital motion, V_{B_0} was [0, 0,7790.6] km/s, that is w-component was very high, which might explain why r-component of the angular velocity is excited the most by mass-actuation. Therefore, not only mass actuation is a factor but the coupling with translational velocity needs to be taken account in orbital motion as well.

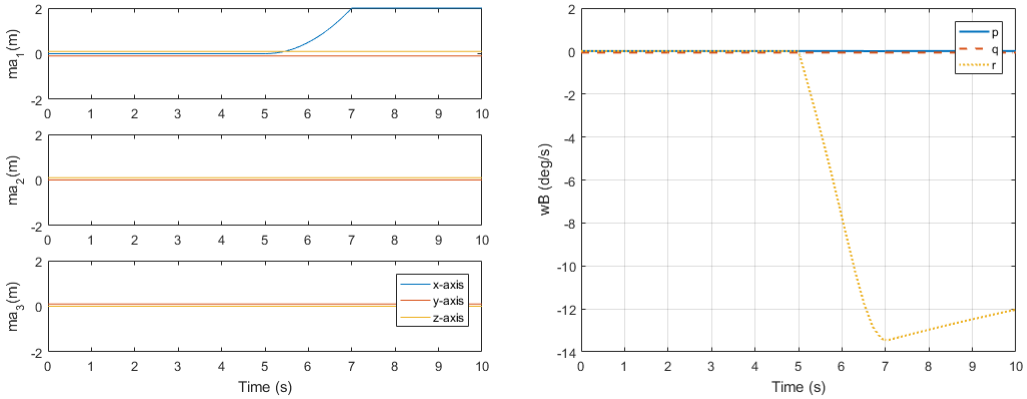

(a) Position of mass actuator (b) ω_B

Figure 3.9: Response when rotational dynamics only with u=[1,0,0]

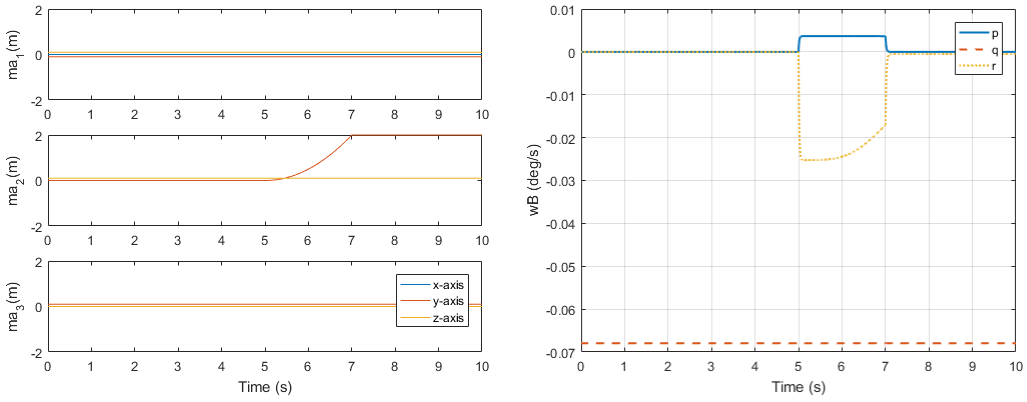

(a) Position of mass actuator (b) ω_B

Figure 3.10: Response when rotational dynamics only with u=[0,1,0]

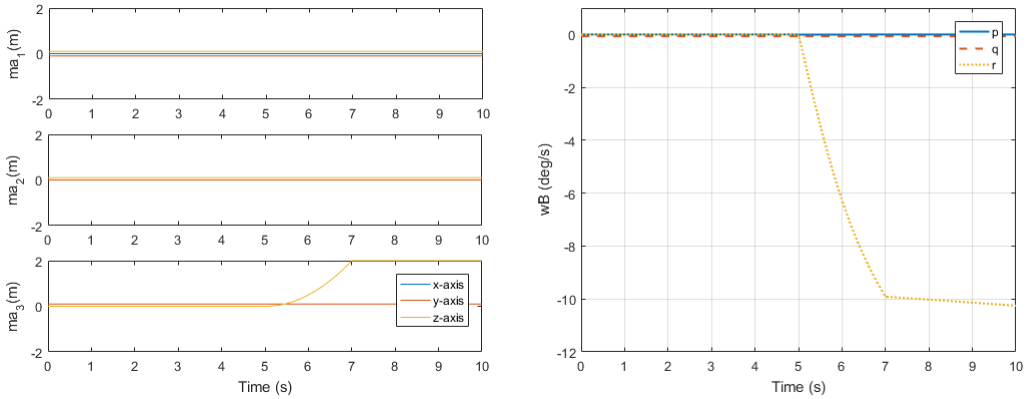

(a) Position of mass actuator (b) ω_B

Figure 3.11: Response when rotational dynamics only with u=[0,0,1]

3.2.3 Full 6-DOF Motion

In this section, the open-loop simulation was carried out with 6-DOF equations of motion. Fig. 3.12 shows that when the ma_1 reached the its position limit, r was not zero so Euler angle kept varying as can be seen in Fig. 3.12 (d). Also, in Fig. 3.12 (a), translational velocity was also changed because it is also coupled with rotational velocity. Since the open-loop does not have a controller, the system does not stay at the nominal condition. It

led to the change in translational velocity significantly. For u=[0, 1, 0] and u=[0, 0, 1], the simulation results were similar to those detailed in Fig. 3.12.

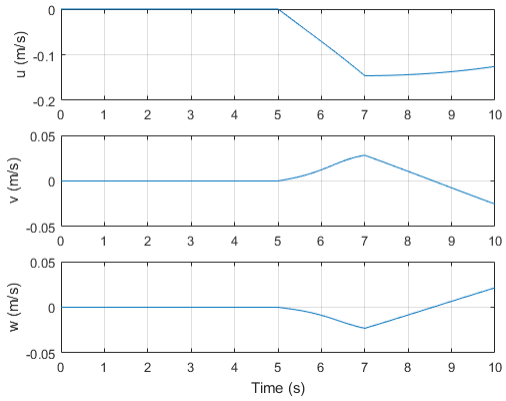

(a) V_B

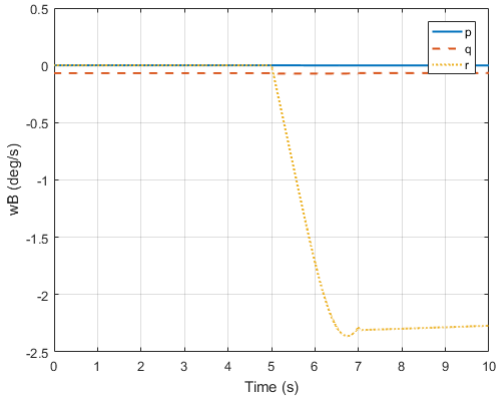

(b) ω_B

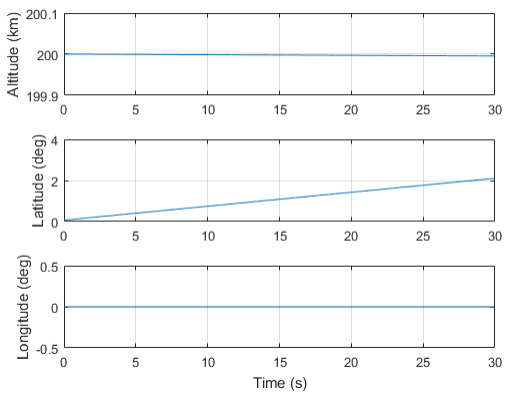

(c) Translational Kinematics

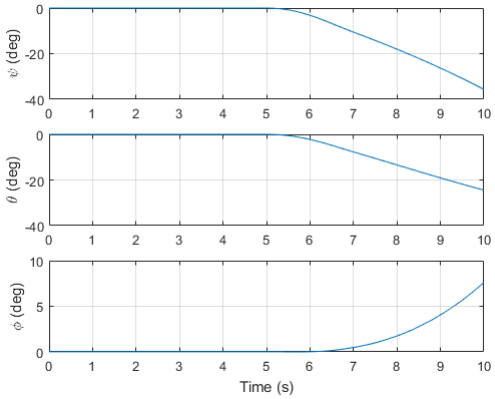

(d) Euler anlges

Figure 3.12: Full 6-DOF motion response when $u = [1,\ 0,\ 0]$

CHAPTER 4

MASS-ACTUATION-BASED CONTROLLER DESIGN FOR DETUMBLING

The control design objective is to bring a tumbling spacecraft into no-rotation or simple spin state using the internal mass motion as the control mechanism. In the equations of motion, the (commanded) acceleration of the three masses are defined as the control input variables. Since the detumbling is the objective, the angular velocity components are defined as the outputs to be controlled.

The control design is carried out using the NDI (Nonlinear Dynamic Inversion) method based on the rotational dynamics equation alone in Eq. (2.12) as this equation relates the output (angular velocity representation) to the control variables (accelerations of the moving masses). The right hand side of the rotational dynamics in Eq. (2.12) is defined as the pseudo control, which leads to

$$\dot{\omega}_B = \nu \tag{4.1}$$

where $\nu = [\nu_p \ \nu_q \ \nu_r]^T$ is

$$\nu = \underline{\underline{\mathbf{I}}}_{\mathbf{t}}^{-1}\{M_B + [\mathbf{S}(\omega_B)\underline{\underline{\mathbf{I}}}_{\mathbf{t}} - \underline{\underline{\dot{\mathbf{I}}}}_{\mathbf{m}}]\omega_B + m_t\mathbf{S}(\rho_{cm,t})\dot{V}_B - m_t\mathbf{S}(\rho_{cm,t})\mathbf{S}(\omega_B)V_B + \sum_{j=1}^{k} m_j\mathbf{S}(\rho_{mj})\ddot{\rho}_{mj}\} \tag{4.2}$$

$$\omega_B = [p \, q \, r]^T \tag{4.3}$$

In scalar form, Eq. (4.1) is

$$\begin{aligned} \dot{p} &= \nu_p \\ \dot{q} &= \nu_q \\ \dot{r} &= \nu_r \end{aligned} \tag{4.4}$$

For each component, a PID (Proportional Integral Derivative) controller is used as

$$\nu_p = K_{P_p}e_p + K_{I_p}\int_0^t e_p d\tau + K_{D_p}\dot{e}_p \tag{4.5}$$

$$\nu_q = K_{P_q}e_q + K_{I_q}\int_0^t e_q d\tau + K_{D_q}\dot{e}_q \tag{4.6}$$

$$\nu_r = K_{P_r}e_r + K_{I_r}\int_0^t e_r d\tau + K_{D_r}\dot{e}_r \tag{4.7}$$

where

$$
\begin{aligned}
e_p &= p_c - p \\
e_q &= q_c - q \\
e_r &= r_c - r
\end{aligned}
\tag{4.8}
$$

Once the linear controllers are designed for the pseudo control variables, the control law for the original control variables should be constructed. This requires the solution of Eq. (4.2) for the original control variables $[\ddot{\rho}_{m_{1x}}\ \ddot{\rho}_{m_{2z}}\ \ddot{\rho}_{m_{3z}}]^T$. These control variables appear in the last term within the summation over j. There are three moving masses in this study, thus $k = 3$. Further, in each $\ddot{\rho}_{mj}$ representation, there is only one component as the others are zero due to the fact that the corresponding mass moves along a single axis. Thus,

$$
\begin{aligned}
&\sum_{j=1}^{3} m_j \mathbf{S}(\rho_{mj}) \ddot{\rho}_{mj} \\
&= m_1 \mathbf{S}(\rho_{m1}) \begin{bmatrix} \ddot{\rho}_{m_{1x}} \\ 0 \\ 0 \end{bmatrix} + m_2 \mathbf{S}(\rho_{m2}) \begin{bmatrix} 0 \\ \ddot{\rho}_{m_{2y}} \\ 0 \end{bmatrix} + m_3 \mathbf{S}(\rho_{m3}) \begin{bmatrix} 0 \\ 0 \\ \ddot{\rho}_{m_{3z}} \end{bmatrix}
\end{aligned}
\tag{4.9}
$$

Carrying out the matrix multiplications and additions in the above equation, and rearranging in terms of the control variables, it can be shown that

$$
\sum_{j=1}^{3} m_j \mathbf{S}(\rho_{mj}) \ddot{\rho}_{mj} = H \begin{bmatrix} \ddot{\rho}_{m_{1x}} \\ \ddot{\rho}_{m_{2y}} \\ \ddot{\rho}_{m_{3z}} \end{bmatrix}
\tag{4.10}
$$

where

$$\mathbf{H} = \begin{bmatrix} 0 & m_2\rho_{m_{2z}} & -m_3\rho_{m_{3y}} \\ -m_1\rho_{m_{1z}} & 0 & m_3\rho_{m_{3x}} \\ m_1\rho_{m_{1y}} & -m_2\rho_{m_{2x}} & 0 \end{bmatrix} \tag{4.11}$$

which should be an invertible matrix, which can be achieved with the right choices of the base positions of the three mass actuators. Rearranging of Eq. (4.2) after substituting Eq. (4.10) leads to the NDI control law for the original control variables as

$$\begin{bmatrix} \ddot{\rho}_{m_{1x}} \\ \ddot{\rho}_{m_{2y}} \\ \ddot{\rho}_{m_{3z}} \end{bmatrix} = \mathbf{H}^{-1}\{\underline{\underline{\mathbf{I}}}_{\mathbf{t}}\nu - M_B - [\mathbf{S}(\omega_B)\underline{\underline{\mathbf{I}}}_{\mathbf{t}} - \dot{\underline{\underline{\mathbf{I}}}}_{\mathbf{m}}]\omega_B + m_t\mathbf{S}(\rho_{cm,t})\mathbf{S}(\omega_B)V_B\} \tag{4.12}$$

Fig. (4.1) depicts the feedback control structure with the implementation of this NDI controller. Here, the state vector (the output of Block S/C) is defined based on Eq. (4.12) as

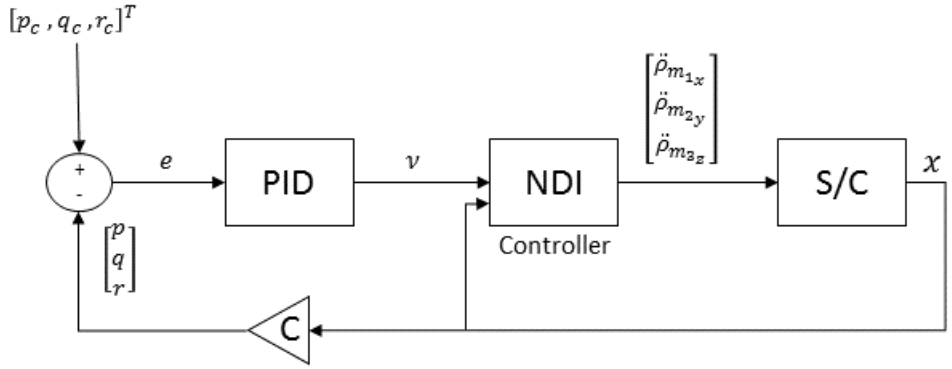

Figure 4.1: NDI+PID feedback control structure

where

$$x = \begin{bmatrix} V_B \\ \omega_B \\ \rho_{m_1} \\ \dot{\rho}_{m_1} \\ \rho_{m_2} \\ \dot{\rho}_{m_2} \\ \rho_{m_3} \\ \dot{\rho}_{m_3} \end{bmatrix} \tag{4.13}$$

and the output matrix is defined as

$$\mathbf{C} = [0_{3\times3} \;\; I_{3\times3} \;\; 0_{18\times3}] \tag{4.14}$$

CHAPTER 5

CLOSED-LOOP SIMULATION

The mass actuated spacecraft was simulated in the MATLAB/Simulink model to examine stabilization of spacecraft under mass actuation using the NDI controller designed in Chapter 4. The detumbling controller is evaluated in closed loop using spacecraft models with increasing fidelity as in Chapter 3.

The spacecraft was tumbling around x, y and z-axis with non-zero p_0, q_0, and r_0. The three mass actuators, ma_1, ma_2 and ma_3 were placed at the initial position and move all the way into the end of its track that measured 4m in length.

5.1 Rotational Dynamics Only

In this section, the simulation investigates the mass actuation on the stationary satellite. More specifically, the spacecraft is not in transational motion but can be in rotational motion by the movement of mass actuators or possible disturbances. Also, the spacecraft is located in deep space so it is not affected by Earth's gravity. For simulation, only the equation of motion of rotational dynamics was used as in Section 3.2.1.

The tumbling condition is that the spacecraft is rotating with p_0= 1 deg/s, q_0= -1 deg/s, and r_0= 0.8 deg/s. To stabilize the spacecraft from tumbling, the commanded output should

be zero. i.e., $p_c = q_c = r_c = 0$.

As shown in the Fig. 5.1, the mass actuator can stabilize the spacecraft when it has no acceleration limits. However, the required acceleration needs to go to as high as $\ddot{\rho}_{m1}$ = [175.5, 0, 0] m/s^2, $\ddot{\rho}_{m2}$ = [0, -129.9, 0] m/s^2, $\ddot{\rho}_{m1}$ = [0, 0, 263.5] m/s^2.

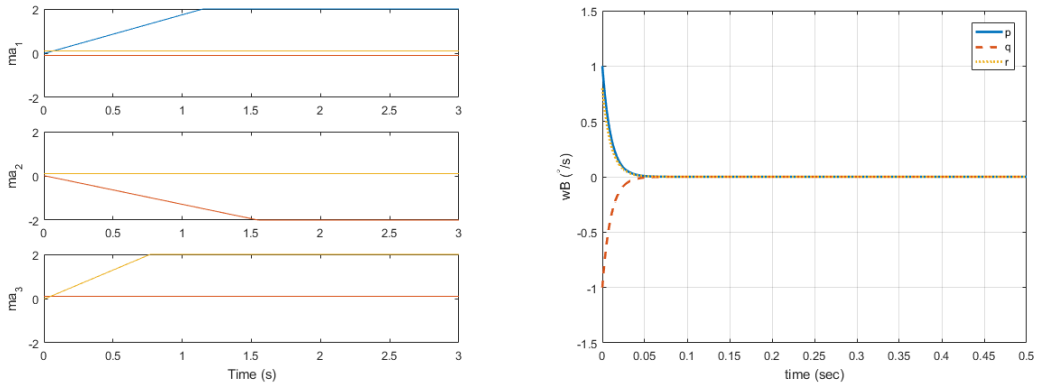

(a) Position of mass actuators

(b) ω_B with no acceleration limit

Figure 5.1: Rotational dynamics response in closed-loop with no acceleration limit

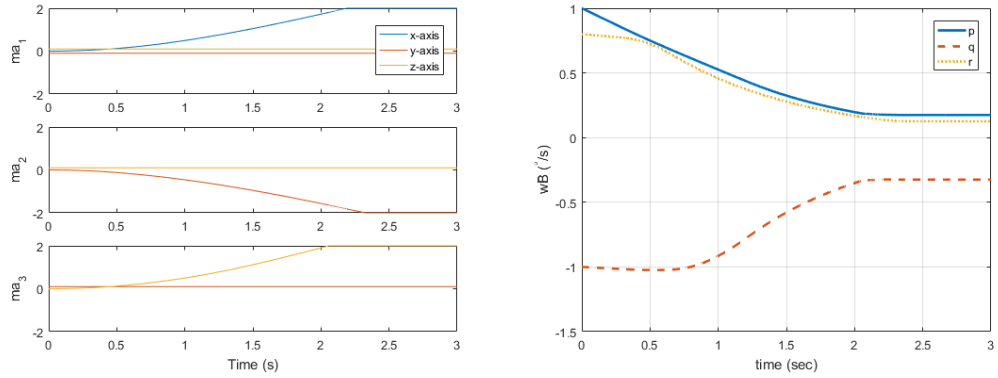

(a) Position of mass actuators

(b) ω_B with $1m/s^2$ of acceleration limit

Figure 5.2: Rotational dynamics response in closed-loop with 1 m/s^2 acceleration limit

Considering the constraints on the mechanisms used to exert acceleration on the mass actuators, there must be an acceleration limit for mass actuators. In the Fig. 5.2, the spacecraft cannot achieve $p_c = q_c = r_c = 0$ when it has $1m/s^2$ of the acceleration limit.

This result presents that the actuators may not always feasible if there is an acceleration limit.

With the acceleration limits imposed, another mechanism to utilize in order to increase the effectiveness of the mass actuators is the offset distances of the mass actuators from the axis along which they move. Thus, in this simulation case, the offset distances are increased from the position 1 to the position 2 as introduced in Section 3.2.1. The position 1 is where ρ_{m1} = [0, -0.1, 0.1] m, ρ_{m2} = [0.1, 0, 0.1] m and ρ_{m3} = [0.1, 0.1, 0] m and the position 2 is where ρ_{m1} = [0, -0.5, 0.5] m, ρ_{m2} = [0.5, 0, 0.5] m and ρ_{m3} = [0.5, 0.5, 0] m. The amount of mass was the same as [40, 40, 40] kg. Increasing distance from the axis caused the increasing moment arms, which tends to increase the inertia force and moment. Fig. 5.3 shows that the mass actuation can successfully stabilizes the spacecraft even with the acceleration limits. This simulation experiment indicates that the various factors that should be considered to vary to improve the closed loop performance include placement of the mass actuators, saturation limits of the acceleration, speed and position, and the amount of mass used in the mass actuators.

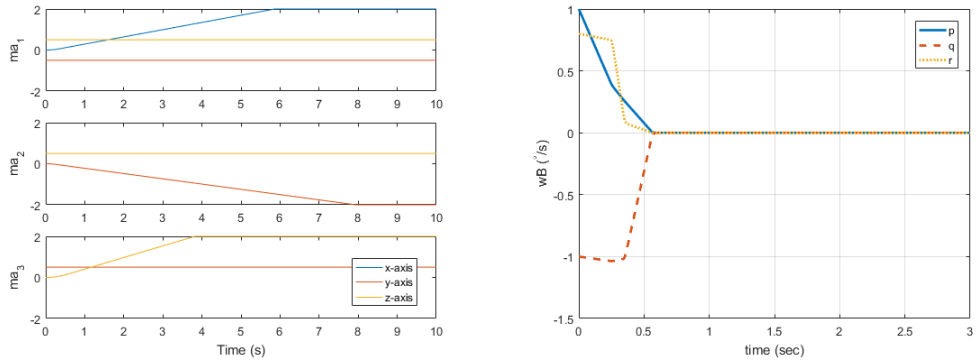

(a) Position of mass actuators (b) ω_B

Figure 5.3: Rotational dynamics response in closed-loop with 1 $/m^2$ limit and position 2

5.2 Rotational Dynamics Coupled with Orbital Motion

In this case, the spacecraft is in the no-spinning nominal case as defined in Section 3.1.1. This simulation case uses only the rotational dynamics equation with the terms representing coupling with the translational motion, as formulated in Eq. (3.3). The translational variables are assumed to stay at their nominal values, i.e. coupling of the translational motion with the rotational motion is ignored while the coupling of the rotational motion with the nominal translational motion is included. This section investigates the performance of the mass actuation in detumbling while the coupling with orbital motion is included in the simulation.

The simulation was conducted with the 40 kg of mass for ma_1, ma_2, and ma_3. Note that, in orbital motion, nominal values for rotational velocity are $p_c = r_c = 0$ and q_c = -0.007 deg/s and translational velocity are $u_0 = v_0 = 0$ and $w_0 = 7790.6\ km/s$.

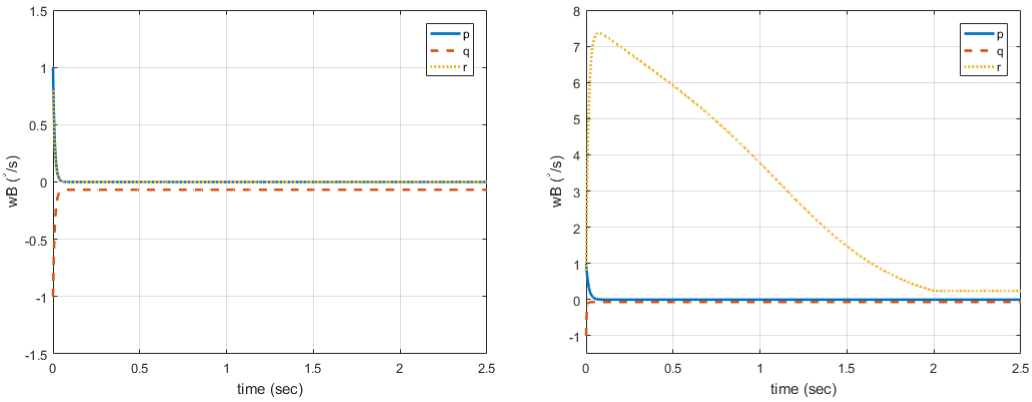

(a) ω_B without an acceleration limit (b) ω_B with an acceleration limit

Figure 5.4: Comparison of ω_B w.r.t acceleration limit

Fig. 5.4 (a) shows that the mass actuator can stabilize the spacecraft when it has no acceleration limits. However, the required accelerations need to go as high as $\ddot{\rho}_{m1}$ = [353.7,

0, 0] m/s^2, $\ddot{\rho}_{m2}$ = [0, 12.31, 0] m/s^2, $\ddot{\rho}_{m1}$ = [0, 0, 133.8] m/s^2. In Fig. 5.4(b), with $\pm 1 m/s^2$ of the acceleration limits, r increased to its peak at 1 second and then decreased but could not converge to zero.

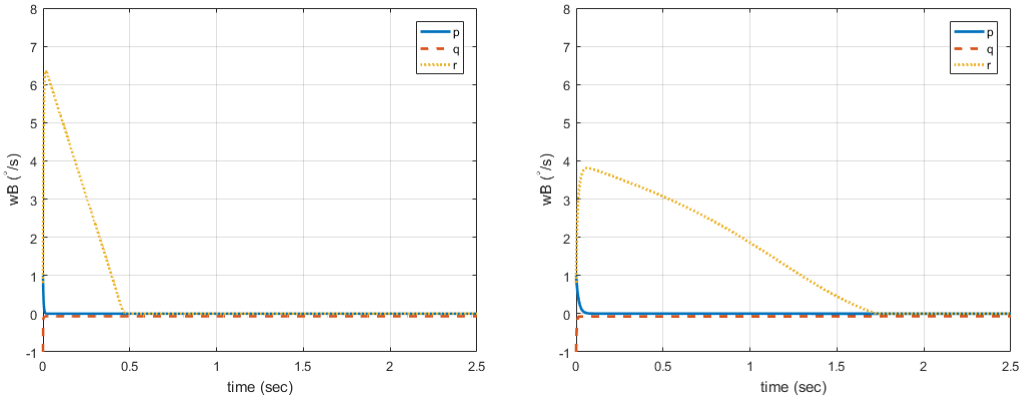

(a) ω_B when position 2 (b) ω_B when ma =[60, 20, 5] (kg)

Figure 5.5: Change in ω_B w.r.t mass and position of the mass actuator

If the amount of mass and/or offset position of the actuator are changed, it can stabilize the system even with acceleration limits. Fig. 5.5 (a) shows that the required detumbling is achieved when the offset distances are increased to the values in the set of position 2, as discussed in Section 5.1. For variation in amount of mass, when the mass of the mass actuators increases, it induces more change in rotational velocity. Fig. 5.5 (b) shows that when ma_1 was the heaviest and ma_3 is the smallest, r_c could be achieved. This results indicates that ma_1 has a decisive effect on the stabilization in r.

The stabilization of r takes longer time than p and q in both simulation cases in Fig. 5.4 and Fig. 5.5. r is the angular velocity around z_B-axis which is the same direction of spacecraft's translational motion. In orbital motion, V_{B_0} was [0 , 0, 7790.6] km/s, which is the reason considered to cause r-component to take longer to stabilize. To better understand the effect of the orbital motion on the stabilization of the spacecraft, the required

accelerations (which is seen when no acceleration limit is imposed) are compared in Fig. 5.6 when the spacecraft is stabilized when only rotational dynamics is considered versus when the spacecraft is coupled with the nominal orbital motion. Fig. 6.6 clearly shows that the required acceleration increases significantly for the masses moving along y- and z-axes while decreases for the mass moving along x-axis when the coupling with the orbital motion is included in the simulation. Especially, the required $\ddot{\rho}_{m1}$, acceleration along x-axis, which has the most effect on r-component, is increased significantly.

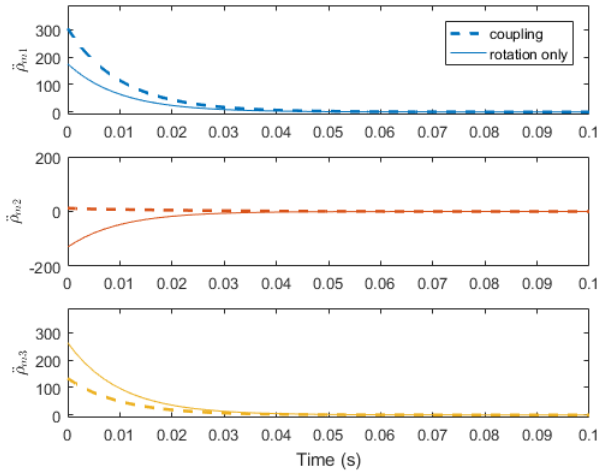

Figure 5.6: Comparision of $\ddot{\rho}_{mj}$ w.r.t. the coupling of orbital motion

5.3 Full 6-DOF Motion

In this section, the full set of equations, rotational and translational dynamics and kinematics, are included in the simulation. This means the cross coupling between the rotational and translational motion as formulated in Eqs. (2.8), (2.12), (2.19), and (2.22) are present and the effects of stabilization of the rotational motion on the orbital motion should be seen.

The simulation was carried out with the $40kg$ of mass for ma_1, ma_2, and ma_3 with acceleration limit of $\pm$ 1 m/s^2. $p_0 = q_0 = r_0 = 0\ deg/s$. The commanded outputs are $p_c = r_c = 0\, deg/s$ and $q_0 = -0.07\ \ deg/s$, which are the nominal values. This simulation is to examine whether the mass actuator control rotational velocity to bring it back to nominal values.

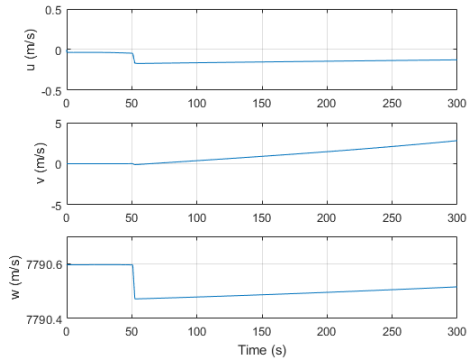

(a) V_B

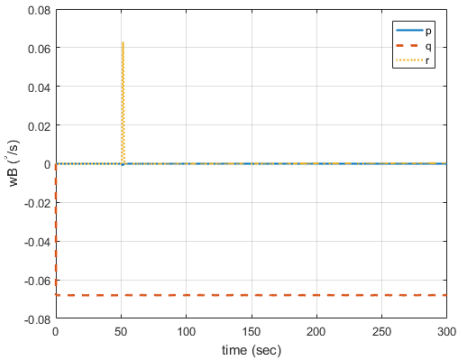

(b) ω_B

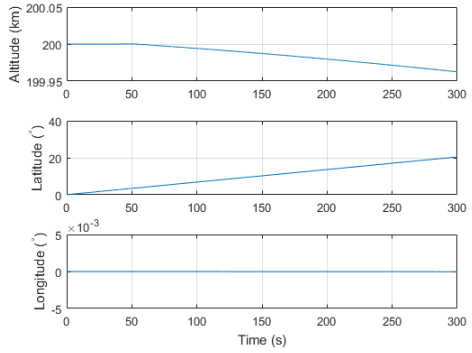

(c) Translation Kinematics

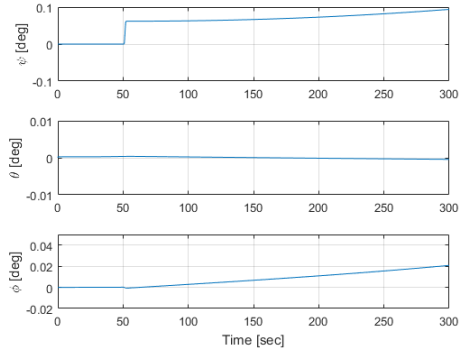

(d) Euler angle w.r.t local frame

Figure 5.7: Full simulation with $\omega_{B_0} = [0, 0, 0] deg/s$

As can be seen in Fig. 5.7(b), q was rapidly decreased to -0.07 deg/s as the nominal value. However, r surged instantly from 0 to 0.06 deg/s at 50 s when ma_2 reaches its position limit, as can be seen in Fig. 5.8. Furthermore, Fig. 5.7 shows that the variation of u, w, altitude and ψ were increased at 50 s. Meanwhile, the effect of the rotational stabilization

on the orbital motion seems to be small until 50 s since u-variation is very small and v- and w-components seem to stay at their respective nominal value. Also, altitude and longitude stayed close to their nominal values as well. After ma_2 position saturates, which is followed by sudden increases to saturation of the other mass actuators at 50 s, the altitude, Euler angles ψ and ϕ start to slowly decrease, and thus deviate from their respective nominal values.

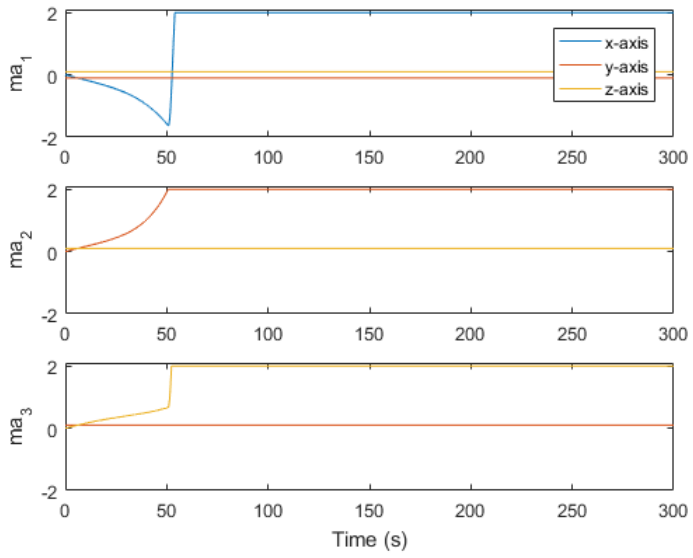

Figure 5.8: Position of mass actuators

The next simulation was conducted with ω_{B_0} which were $p_0 = 1\ deg/s$, r_0 = -1 deg/s and $q_0 = 0.8\ deg/s$. This initial values represent more severe disturbance than previous simulation shown in Fig. 5.7. During this simulation, Fig. 5.9 (a) shows that the translational velocity was changed due to the coupling with rotational dynamics. Also, in the Fig. 5.9 (c) and (d), the altitude and orientation was affected by the change in rotational velocity. In this simulation, the result indicates that while the mass actuator controls the rotational velocity, the dynamics and kinematics are changed unavoidably due to the cross coupling

each other.

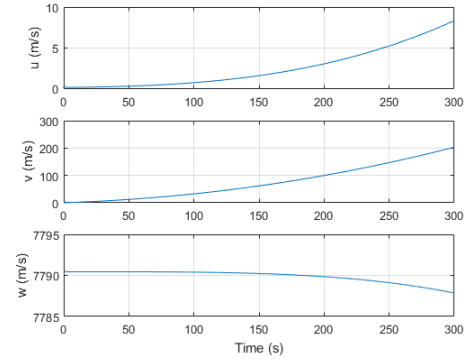

(a) V_B

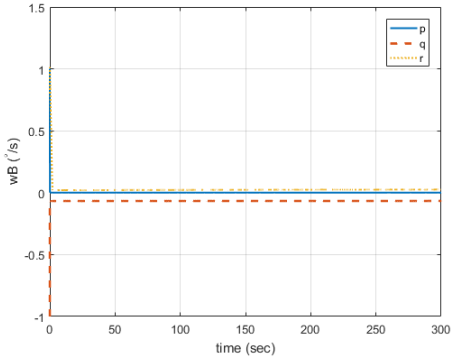

(b) ω_B

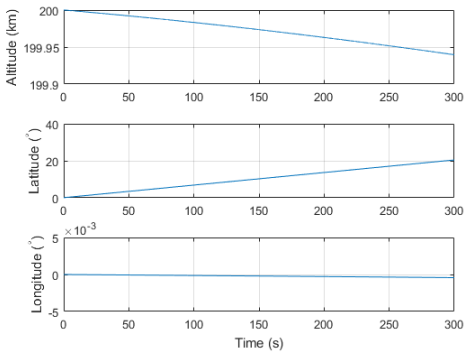

(c) Translational Kinematics

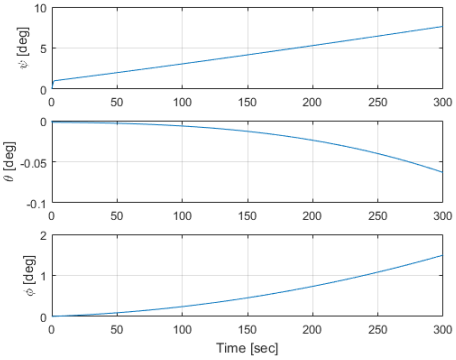

(d) Euler angles

Figure 5.9: Full simulation with $\omega_{B_0} = [1, -1, 0.8] deg/s$

CHAPTER 6

CONCLUSION

This research investigates the ability of stabilizing spacecraft rotational motion by internal mass actuation. The mass actuation mechanism consists of three internal masses placed along the three axes at some offset distance that can move to induce inertial forces and moments and change the inertia matrix and center of mass. Results indicated that the mass actuators was feasible for detumbling the spacecraft which was traveled in deep space or in a circular orbit.

A set of nonlinear equations of motion are developed to model the motion, both orbital and rotational dynamics and kinematics, of a spacecraft with mass and inertial variation due to internal mass actuation, under the gravitational field of Earth. The equations inherently include the inertia effect of the mass motion on the orbital and rotational dynamics. Translational kinematics is written in terms of altitude, longitude and latitude, and the rotational kinematics is expressed relative to the local horizontal and local vertical frame.

In this study, the application of mass actuators was simulated and examined in phases. The equations of motion were first used to analyze two nominal flight conditions: (1) spacecraft facing towards Earth on a circular orbit, and (2) spacecraft spinning around the axis towards Earth on a circular orbit. The open-loop system provided the rotational dynamics

response of mass actuated spacecraft.

A NDI (Nonlinear Dynamic Inversion) based controller was designed to stabilize the spacecraft by mass actuation in the first nominal condition from a tumbling condition. This controller was evaluated at three levels in terms of the fidelity of the spacecraft model: (1) only rotational dynamics equations, (2) rotational dynamics coupled with the nominal orbital motion, and (3) the full nonlinear 6-DOF model.

In the first case, the simulation was carried out with the rotational dynamics only. Due to the absence of gravity effect and translational velocity, the change in the rotational velocity was induced by the motion of mass actuators. The spacecraft was assumed to be tumbling around x, y, and z-axis. Without the acceleration limits of mass actuators, the spacecraft achieved the stabilization. However, when there was an acceleration limit, the spacecraft could not stabilize all components of rotational velocity when the mass amounts are small and the offset distances are short. In severe disturbance like three axes tumbling, the mass actuator may not be feasible due to its limits. It was shown, however, that when the mass amounts are increased and/or the offset distances are increased, the effectiveness of mass-actuation increases and thus the stabilization is still possible even with acceleration limits.

In the second case, the spacecraft stays in the circular orbit (constant speed, always facing Earth) regardless of the rotational motion. This is because the rotational dynamics with the coupling terms with the translational motion is used. The simulation results showed the effect of the orbital motion on the stabilization of the rotational motion. The simulation results show that the stabilization of the rotational motion is obtained although the decrease in the disturbance along z-axis has taken longer time than the disturbances along other axes. This is because the spacecraft was in translational motion with high speed of [0, 0, 7990.6]

m/s. Furthermore, for control r, ma_1 was the most effective control variable.

In the last case, it was shown that the angular velocity can be returned to the nominal condition using mass actuation even when the full nonlinear equations of motion are considered, which models cross coupling between the rotational and translational motion. In the meantime, the control of the rotational motion had some effect on the orbital motion, specifically the translational velocity components, and also the orientation of the spacecraft.

The main original contribution of this thesis is the consideration of the orbital motion along with the rotational motion when studying detumbling with mass actuation. Most prior research efforts do not consider the orbital motion in their system while using moving mass to control the attitude or rotational velocity or maneuver. They usually consider the rotational dynamics only. In order to apply this concept to the spacecraft in Earth orbit, the orbital motion must be included. Also, some of them show they do not control full 3-axes of attitude or rotational velocity.

The thesis presents that the mass actuators is feasible for deep space satellite and low Earth orbit satellite. Also, it can stabilize from any 3-axes disturbance. There might be a benefit from the mass actuator for an extension of its lifespan by not using thrusts or high energy consuming actuators. Furthermore, it can be an alternative mean for a failure of primary actuators.

For future work, the simulation results showed that after detumbling, the spacecraft's translational velocity and orientation were changed. This is because the mass actuators control the rotational velocity, not control the attitude of spacecraft. Therefore, the future subject of study would be the attitude control with mass actuation. Furthermore, it is necessary to see whether the mass actuator can control the spacecraft's attitude as a main actuator of the spacecraft.

Appendix A

TRANSFORMATION FROM EARTH-FIXED FRAME TO LOCAL FRAME

The position of a spacecraft orbiting around Earth is usually expressed in terms of altitude, latitude, and longitude. This section explains the procedure to obtain the relation between these parameters and the position of the spacecraft in Earth-fixed frame. This procedure involves two reference frames: (1) Earth-fixed frame, and (2) Local-horizontal-local-vertical, or "local" in short, frame.

Earth-fixed frame is defined such that (1) the origin is at the center of Earth, (2) z-axis, z_E, is points towards the North pole, (3) x_E-axis is towards the point on the surface coinciding the latitude of 0 deg (Equator) and the longitude of 0 deg (Greenwich), and (4) y_E-axis is normal to x_E-z_E plane to complete the right handed Cartesian coordinate system.

Local frame is defined such that its x-axis always points at the spacecraft. Thus, position of the spacecraft is always along the x-axis of the local frame. Thus, the position vector of the spacecraft is written in local frame as

$$\underline{r}_B = [L]^T \begin{bmatrix} R+h \\ 0 \\ 0 \end{bmatrix} \tag{A.1}$$

where $[L]$ is the vectrix of the local frame, R is the radius of Earth, and h is the altitude of the spacecraft, as depicted in Fig. A.1.

To express the position vector in Earth-fixed frame, the rotation matrix from Earth-fixed frame to local-frame should be used. The local frame is defined such that its orientation with respect to Earth-fixed frame is obtained through two elementary rotation: (1) rotation around z_E-axis by angle of L degree, where L is "the longitude" by definition, and (2) rotation around the new y-axis in the negative direction by angle λ, which is "the latitude" by definition.

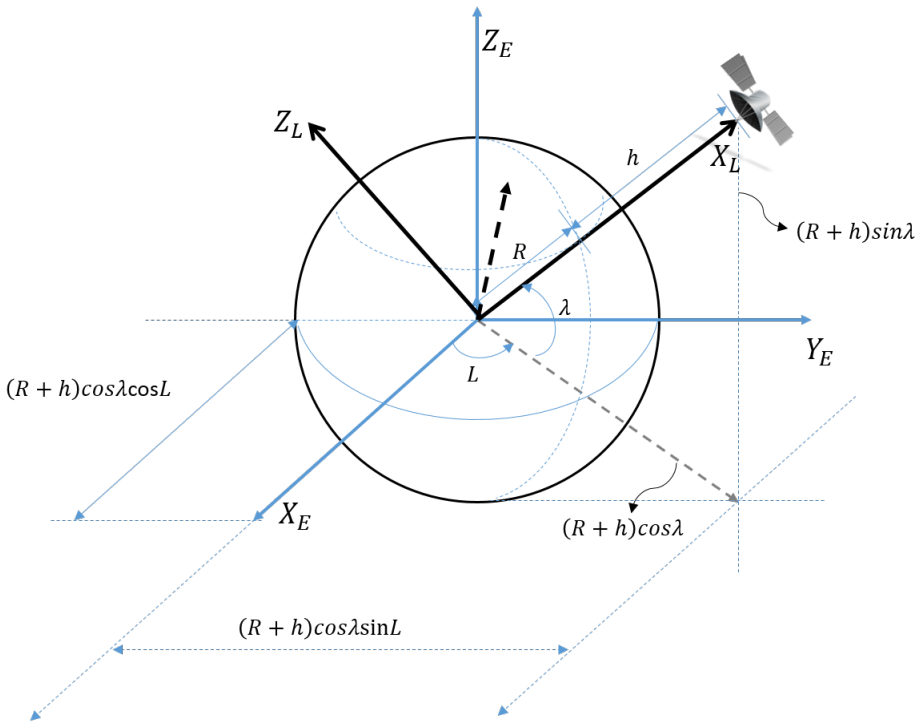

Figure A.1: Depiction of Earth-fixed and local frame

Recall that the standard rotation matrix in terms of Euler angles, (ψ, θ, ϕ) is obtained through 321 elementary rotations, i.e., (1) rotation around z-axis by angle ψ, (2) rotation around y-axis by angle θ, and (3) rotation around x-axis by angle ϕ as

$$\mathbf{R_{BL}} = \begin{bmatrix} cos\psi cos\theta & cos\theta sin\psi & -sin\theta \\ -cos\phi sin\psi + sin\phi sin\theta cos\psi & cos\phi cos\psi + sin\phi sin\theta sin\psi & sin\phi cos\theta \\ sin\theta sin\psi + cos\phi sin\theta cos\psi & -sin\phi cos\psi + cos\phi sin\theta sin\psi & cos\phi cos\theta \end{bmatrix} \tag{A.2}$$

Since the rotation from Earth-fixed to local frame involves elementary rotations around 3^{rd} axis, and then 2^{nd} axis, the standard rotation matrix, given in Eq. (A.1), in terms of 321 Euler angles, can be used to obtain the rotation matrix from Earth-fixed to local frame. This is done by simply replacing ψ with L, θ with $-\lambda$, and setting $\phi = 0$ as no third rotation

is needed, which leads to

$$\mathbf{R_{LI}} = \begin{bmatrix} cos\lambda cosL & cos\lambda SinL & sin\lambda \\ -sinL & cosL & 0 \\ -sin\lambda cosL & -sin\lambda sinL & cos\lambda \end{bmatrix} \tag{A.3}$$

Appendix B

NOMINAL CONDITION ANALYSIS

This section describes the procedure for determining the conditions for control variables and values for the state variables in a specified nominal flight condition. The nominal values obtained through such an analysis are used to run a dynamic simulation by initializing the state variables to their nominal values and setting the control variables at their nominal values as the first step of verifying the accuracy of the dynamic simulation. The nominal values of the state and control variables are also used when a linear model is to be derived for a given nonlinear model. Nominal values of state and control variables are also used to initialize nonlinear dynamic simulations. The specific nominal condition analyzed in this section is as follows. The spacecraft travels in a circular orbit with constant translational speed. Circular orbit implies that altitude is constant, i.e., $h = h_0$, and $\dot{h} = 0$. At the same time, the spacecraft points towards Earth and spinning around the direction towards Earth. More specifically, the x-axis of the spacecraft body frame is always aligned with x-axis of the local frame while the spacecraft rotates around the x-axes with a constant speed. Further, the circular orbit is chosen to be in a vertical plane corresponding to the longitude of 0 deg, which implies $L = \dot{L} = 0$. During a nominal condition flight, the internal masses are considered to be stationary at specified location, which implies $\dot{\rho}_{m_j} = \ddot{\rho}_{m_j} = 0$.

Consider that ψ, θ, ϕ are the Euler angles of the spacecraft relative to the local frame. Also, note that x_B-axis is aligned with x_L-axis, which implies that $\psi = \theta = 0$ during the nominal flight. Thus, the rotation matrix in the nominal condition is

$$\mathbf{R_{BL}} = \begin{bmatrix} 1 & 0 & 0 \\ 0 & cos\phi & sin\phi \\ 0 & -sin\phi & cos\phi \end{bmatrix} \tag{B.1}$$

The nominal longitude is selected to be $L = 0$, which further implies that $\dot{L} = 0$. Thus,

the rotation matrix from the inertial frame to the local frame becomes

$$\mathbf{R_{LI}} = \begin{bmatrix} cos\lambda & 0 & sin\lambda \\ 0 & 1 & 0 \\ -sin\lambda & 0 & cos\lambda \end{bmatrix} \tag{B.2}$$

Similarly , matrix ϵ becomes

$$\boldsymbol{\epsilon} = \begin{bmatrix} cos\lambda & -(R+h_0)sin\lambda & 0 \\ 0 & 0 & (R+h_0)cos\lambda \\ sin\lambda & (R+h_0)cos\lambda & 0 \end{bmatrix} \tag{B.3}$$

Since altitude h and longitude L are constant,

$$\dot{\chi} = \begin{bmatrix} 0 \\ \dot{\lambda} \\ 0 \end{bmatrix} \tag{B.4}$$

Translational velocity vector in the body frame is expressed as

$$V_B = \begin{bmatrix} u \\ v \\ w \end{bmatrix} \tag{B.5}$$

Rewriting the translational kinematics in, Eq.(2.19), gives

$$\boldsymbol{\epsilon}\dot{\chi} = \mathbf{R}_{\mathbf{LI}}^T \mathbf{R}_{\mathbf{BL}}^T V_B \tag{B.6}$$

Putting the matrix expansions introduced above in this form of the translational kine-

matics yields

$$-\dot{\lambda}(R+h_0)sin\lambda = ucos\lambda - sin\lambda(vsin\phi + wcos\phi) \tag{B.7}$$

$$0 = vcos\phi - wsin\phi \tag{B.8}$$

$$\dot{\lambda}(R+h_0)cos\lambda = vsin\lambda + cos\lambda(vsin\phi + wcos\phi) \tag{B.9}$$

Eq.(B.7) and Eq.(B.9) are rewritten by dividing them by $sin\lambda$ and $cos\lambda$, respectively

$$-\dot{\lambda}(R+h_0) = \frac{ucos\lambda}{sin\lambda} - (vsin\phi + cos\phi) \tag{B.10}$$

$$-\dot{\lambda}(R+h_0) = \frac{usin\lambda}{cos\lambda} + vsin\phi + cos\phi \tag{B.11}$$

Adding these two equations together leads to

$$0 = \frac{u}{sin\lambda cos\lambda} \tag{B.12}$$

which implies $u = 0$ for any λ. With $u = 0$, either Eq.(B.10) and (B.11) leads to

$$\dot{\lambda} = \frac{vsin\phi + wcos\phi}{R+h} \tag{B.13}$$

Eq.(B.8) implies

$$tan\phi = \frac{v}{w} \tag{B.14}$$

which implies

$$sin\phi = \frac{v}{V} \tag{B.15}$$

$$cos\phi = \frac{w}{V} \tag{B.16}$$

where $V = \sqrt{v^2 + w^2}$, the magnitude of the orbital velocity of the spacecraft since $u = 0$. Substituting Eq.(B.15) and (B.16) into Eq.(B.13) gives

$$\dot{\lambda}_0 = \frac{V}{R + h_0} \tag{B.17}$$

Using Eq.(B.15) and (B.16), and the fact that $u = 0$, the translational velocity, as represented in the body frame, can be written as

$$V_B = \begin{bmatrix} 0 \\ Vsin\phi \\ Vcos\phi \end{bmatrix} \tag{B.18}$$

where note that y- and z-components are time-varying through ϕ and V is not constant in this general nominal flight condition.

Recall that $\psi = \theta = 0$ and $\dot{\phi} = p_0$, a constant in the nominal condition. Under these conditions, rotational kinematics in ,Eq. (2.21), written in terms of the Euler angles of the spacecraft body frame relative to the local frame, leads to

$$0 = w_y sin\phi + w_z cos\phi \tag{B.19}$$

$$0 = w_y cos\phi - w_z sin\phi \tag{B.20}$$

$$p_0 = w_x \tag{B.21}$$

which implies $w_x = p_0$, $w_y = 0$, $w_z = 0$. That is, the angular velocity with respect to the local frame, expressed in the body frame is,

$$\omega_{BL} = \begin{bmatrix} p_0 \\ 0 \\ 0 \end{bmatrix} \tag{B.22}$$

The angular velocity of the local frame with respect to the inertial frame, when $\dot{L} = 0$, in the nominal condition, is reduced to

$$\omega_L = \begin{bmatrix} 0 \\ -\dot{\lambda} \\ 0 \end{bmatrix} \tag{B.23}$$

The angular velocity of the body frame with respect to the inertial frame is formulated from Eq. (B.22) and (B.23), in the nominal condition, as

$$\omega_B = \omega_{_{BL}} + \mathbf{R_{BL}}\omega_L = \begin{bmatrix} p_0 \\ -\dot{\lambda}cos\phi \\ \dot{\lambda}sin\phi \end{bmatrix} \tag{B.24}$$

Note that, y and z components are time dependent as $\dot{\phi} = p_0$ and thus ϕ varies linearly with time.

The internal mass actuators are stationary in this nominal condition, which reduces the

translational dynamics in ,Eq. (2.8), to

$$\dot{V}_B = \frac{1}{m_t} F_{B_R} - \mathbf{S}(\rho_{cm,t})\dot{\omega}_B + \mathbf{S}(\omega_B) - \mathbf{S}^2(\omega_B)\rho_{cm,t} \tag{B.25}$$

where the external force, in the nominal condition, is expressed as

$$F_B = \begin{bmatrix} -m_t \dfrac{\mu}{(R+h_0)^2} \\ 0 \\ 0 \end{bmatrix} + \begin{bmatrix} F_x \\ F_y \\ F_z \end{bmatrix} \tag{B.26}$$

where F_x, F_y, F_z are components in the body frame of the applied force due to external sources other than gravity such as thruster.

$$\dot{\omega}_B = \begin{bmatrix} 0 \\ p_0 \dot{\lambda} sin\phi \\ p_0 \dot{\lambda} cos\phi \end{bmatrix} \tag{B.27}$$

$$\rho_{cm,t} = \begin{bmatrix} \rho_{cm,tx} \\ \rho_{cm,ty} \\ \rho_{cm,tz} \end{bmatrix} \tag{B.28}$$

Note also that x-component of $\dot{V}_B$ is zero since u, x-component of V_B, is constant as shown earlier.

Then, the first row of Eq.(B.25) gives

$$0 = -\frac{\mu}{(R+h_0)^2} + F_x - 2\dot{\lambda}_0 p_0 \rho_{cm,t_z} sin\phi + 2\dot{\lambda}_0 p_0 \rho_{cm,t_y} cos\phi + \dot{\lambda}_0 V + \dot{\lambda}^2 \rho_{cm,t_x} \tag{B.29}$$

Substituting $\dot{\lambda}_0$ from Eq.(B.17) in this equation, and rearranging lead to a quadratic equation for V as

$$V^2 + 2p_0(-\rho_{cm,t_z} sin\phi + \rho_{cm,t_y} cos\phi)\frac{R+h_0}{R+h_0+\rho_{cm,t_x}}V + \frac{F_x}{m_t}\frac{(R+h_0)^2}{(R+h_0+\rho_{cm,t_x})} - \frac{\mu}{R+h_0+\rho_{cm,t_x}} = 0 \tag{B.30}$$

This equation can be analyzed in two cases depending on whether $F_x = 0$. When $F_x = 0$, Eq. (B.30) becomes

$$V^2 + 2p_0(-\rho_{cm,t_z} sin\phi + \rho_{cm,t_y} cos\phi)\frac{R+h_0}{R+h_0+\rho_{cm,t_x}}V - \frac{\mu}{R+h_0+\rho_{cm,t_x}} = 0 \tag{B.31}$$

where note that the coefficient of the linear term is time-varying through ϕ, which implies V_0, the nominal value of V, is also time-varying even in the nominal condition. The linear term also indicates the special cases where V is constant

(1) When p_0, no spinning around x_B-axis.

(2) When the moving masses are placed in such a way that $\rho_{cm,t_y} = \rho_{cm,t_z} = 0$.

In either case,

$$V = \pm\sqrt{\frac{\mu}{R+h_0+\rho_{cm,t_x}}} \tag{B.32}$$

which is now constant when ρ_{cm,t_x} is kept constant. This implies, from Eq.(B.17) that $\dot{\lambda}_0$ is also constant.

When none of the above special cases is present, the linear term in Eq.(B.30) can be removed by properly selecting F_x as

$$F_{x_0} = 2\frac{m_t p_0}{R+h_0}(\rho_{cm,t_z} sin\phi - \rho_{cm,t_y} cos\phi)V_0 \tag{B.33}$$

where note that F_{x_0}has to be time-varying due to ϕ. When $F_x = F_{x_0}$, $V = V_0$, a constant, as formulated in Eq. (2.12), even when p_0, ρ_{cm,t_y} and ρ_{cm,t_z} are not zero.

In the case of constant V_0, the other two components of Eq.(B.32) are used to derive the formulation of y and z-components of the applied force as

$$\begin{bmatrix} F_{y_0} \\ F_{z_0} \end{bmatrix} = -m_t \dot{\lambda}_0^2 \begin{bmatrix} sin^2\phi & sin\phi cos\phi \\ sin\phi cos\phi & cos^2\phi \end{bmatrix} \begin{bmatrix} \rho_{cm,t_y} \\ \rho_{cm,t_z} \end{bmatrix} \tag{B.34}$$

which shows that F_{y_0} and F_{z_0} are also time-varying due to ϕ.

In the nominal condition studied where the mass actuators are stationary, the rotational dynamics in Eq.(2.12) reduces to

$$\dot{\omega}_B = \underline{\underline{\mathbf{I}}}_{\mathbf{t}}^{-1}\{M_B + \mathbf{S}(\omega_B)\underline{\underline{\mathbf{I}}}_{\mathbf{t}}\omega_B + m_t\mathbf{S}(\rho_{cm,t})\dot{V}_B - m_t\mathbf{S}(\rho_{cm,t})\mathbf{S}(\omega_B)V_B\} \tag{B.35}$$

where the total external moment is

$$M_B = M_{B_G} + \tau_B \tag{B.36}$$

where M_{B_G} is the moment due to the gravity and can be expressed in the nominal condition considered as

$$M_{B_G} = m_t\mathbf{S}(\rho_{cm,t}) \begin{bmatrix} \dfrac{\mu}{(R+h)^2} \\ 0 \\ 0 \end{bmatrix} \tag{B.37}$$

and τ_B is the applied torque from a source other than the mass actuation, such as control moment gyro and thrusters.

In the general nominal case, recall that

$$\omega_{B_0} = \begin{bmatrix} p_0 \\ -\dot{\lambda}_0 cos\phi \\ \dot{\lambda}_0 sin\phi \end{bmatrix} \tag{B.38}$$

$$\dot{\omega}_{B_0} = \begin{bmatrix} p_0 \\ \dot{\lambda}_0 p_0 sin\phi \\ \dot{\lambda}_0 p_0 cos\phi \end{bmatrix} \tag{B.39}$$

$$V_{B_0} = \begin{bmatrix} 0 \\ V sin\phi \\ V cos\phi \end{bmatrix} \tag{B.40}$$

$$\dot{V}_{B_0} = \begin{bmatrix} 0 \\ \dot{V} sin\phi + V p_0 cos\phi \\ \dot{V} cos\phi - V p_0 sin\phi \end{bmatrix} \tag{B.41}$$

It is clear from Eq.(B.35) that to sustain this general nominal condition, there should be applied torque as

$$\tau_{B_0} = \underline{\underline{\mathbf{I}}}_{\mathbf{t}} \dot{\omega}_{B_0} - M_{B_G} - \mathbf{S}(\omega_B) \underline{\underline{\mathbf{I}}}_{\mathbf{t}} \omega_{B_0} - m_t \mathbf{S}(\rho_{cm,t}) \dot{V}_{B_0} + m_t \mathbf{S}(\rho_{cm,t}) \mathbf{S}(\omega_{B_0}) V_{B_0} \tag{B.42}$$

where note that τ_B is time-varying through time varying ω_{B_0} and V_{B_0}. In the special

nominal case with $p_0 = 0$ and V_0 constant

$$\omega_B = \begin{bmatrix} 0 \\ -\dot{\lambda}_0 \\ 0 \end{bmatrix} \tag{B.43}$$

$$\dot{\omega}_B = \begin{bmatrix} 0 \\ 0 \\ 0 \end{bmatrix} \tag{B.44}$$

$$V_B = \begin{bmatrix} 0 \\ 0 \\ V_0 \end{bmatrix} \tag{B.45}$$

$$\dot{V}_B = \begin{bmatrix} 0 \\ 0 \\ 0 \end{bmatrix} \tag{B.46}$$

where $\phi_0 = 0$ is chosen. In this case, the applied torque becomes constant as

$$\tau_{B_0} = -M_{B_0} - \mathbf{S}(\omega_{B_0})\underline{\underline{\mathbf{I}}}_{\mathbf{t}}\omega_{B_0} - m_t\mathbf{S}(\rho_{cm,t})\mathbf{S}(\omega_{B_0})V_{B_0} \tag{B.47}$$

Furthermore, when $\rho_{cm,t} = 0$, $M_{B_G} = 0$ by Eq. (B.37). In this special case

$$\tau_{B_0} = -M_{B_0} - \mathbf{S}(\omega_{B_0})\underline{\underline{\mathbf{I}}}_{\mathbf{t}}\omega_{B_0} = \begin{bmatrix} -I_{yz}\dot{\lambda}_0^2 \\ 0 \\ -I_{xy}\dot{\lambda}_0^2 \end{bmatrix} \tag{B.48}$$

where I_{yz} and I_{xy} are products of inertia in matrix $\underline{\underline{\mathbf{I}}}_{\mathbf{t}}$. This implies that no applied torque is required in this special case when $I_{xy} = I_{yz} = 0$

REFERENCES

[1] Kunciw, B. G. "Optimal Detumbling of a Large Manned Spacecraft Using an Internal Moving Mass". 1, June, 1973.

[2] Lewin, S. "Video Shows Japan's Hitomi Satellite Tumbling in Space, Rescue Efforts Underway", 2016.

[3] Erturk, S. A. and Dogan, A. "Propeller Torque Effect on Cruise Trim of Standard and Mass-Actuated Airplane Supplied voltage", June, 2015, pp. 1–17.

[4] Erturk, S. A. and Dogan, A. "Trim Analysis of a Moving-mass Actuated Airplane in Steady Turn". *51st AIAA Aerospace Sciences Meeting including the New Horizons Forum and Aerospace Exposition*, January, 2013, pp. 1–12.

[5] Menon, P. K., Sweriduk, G. D., Ohlmeyer, E. J., and Malyevac, D. S. "Integrated guidance and control of moving-mass actuated kinetic warheads". *Journal of Guidance, control, and Dynamics* 27.1, 2004, pp. 118–126.

[6] Yao, Y. and Jiang, Y. "Attitude Stabilization of Spacecraft with Two Moving-Mass Via Interconnection and Damping Assignment". *2008 chinese Control and Decision Conference*, 2008, pp. 5115–5118.

[7] Bean, J. "Small Satellite Attitude Control Using Linear Moving", April, 2010.

[8] Dev Kumar, K. and Zou, A.-M. "Attitude Control of Miniature Satellites Using Movable Masses". *Spaceops*, 2010.

[9] Jiang, Y., Zheng, K., and Yang, B. "Attitude control design of underactuated mass moment spacecraft based on nonsmooth Lipschitz surface". *33rd Chinese Control Conference, CCC 2014*, July, 2014, pp. 43–48.

[10] Ahn, Y. T. "Attitdue Dynamics and Control of a Spacecraft Using Shifting Mass Distribution". Dissertation. The Pennsylvania State University, State College, PA, 2012.

[11] Kunciw, B. G. and Kaplan, M. H. "Optimal Space Station Detumbling by Internal". *Automatica* 12, 1976, pp. 417–425.

[12] Dogan, A. and Blake, W. "Flight Mechanics of Aerial Refueling Mathematical Modeling and Simulation", 2015.

[13] Jiang, Y., Fenghua, H., and Yao, Y. "Hybrid Control Strategy for Attitude Stabilization of an Underactuated Spacecraft with Two Moving Mass". *IEEE International Conference on Automation and Logistics*, August, 2007, pp. 389–393.

[14] Erturk, S. A. and Dogan, A. "Controllability Analysis of a Mass-Actuated Airplane". *AIAA Atmospheric Flight Mechanics Conference*, January, 2015, pp. 1–14.

[15] Kim, E. "Control and Simulation of Relative Motion for Aerial Refueling in Racetrack Maneuver". MSAE thesis. University of Texas at Arlington, Arlington TX, May, 2007.

[16] Lewis, T. A. "Flight Data Analysis and Simulation of Wind Effects During Aerial Refueling". MSAE thesis. University of Texas at Arlington, Arlington, TX, May 2008.

[17] Erturk, S. A. "Trimming Mass-Actuated Airplane in Turns with Zero Side Slip Angle". *AIAA Atmospheric Flight Mechanics Conference*, January, 2014.

[18] Chun, H. K. "Pitch Stabilization of Satellite us ing Nonlinear Controller". MS thesis. KyungHee University, Feburary, 2000.

[19] Weck, O. L. D. "Attitude Determination and Control (Adcs)", 2001, pp. 1–57.

[20] Kim, J. J. and Agrawal, B. N. "Automatic Mass Balancing of Air-Bearing-Based Three-Axis Rotational Spacecraft Simulator". *Journal of Guidance, Control, and Dynamics* 32.3, June, 2009, pp. 1005–1017.

[21] Kumar, K. D. and Zou, A.-M. "Attitude Control of Miniature Satellites Using Movable Masses". *Spaceops 2010 Conference*, April, 2010.

[22] Chesi, S., Gong, Q., Pellegrini, V., Cristi, R., and Romano, M. "Automatic Mass Balancing of a Spacecraft Three-Axis Simulator: Analysis and Experimentation". *Journal of Guidance, Control, and Dynamics* 37.1, 2014, pp. 197–206.

[23] Hwang, H. "ParametricAnalysisforSystem ConceptualDesign ofHighAgility SmallObservationSatellite". MS thesis. Korea Aerospace University, Feburary, 2012.

[24] Edwards, T. L. and Kaplanf, M. H. "Automatic Spacecraft Detumbling by Internal Mass Motion". *AIAA Journal* 12.4, 1974, pp. 496–502.

[25] Yuan, Z., Jianping, X., Jin, J., and Jian, Y. "Stabilization analysis and algorithm refactoring of underactuated small satellite using two wheels". *2013 25th Chinese Control and Decision Conference, CCDC 2013*, 2013, pp. 2314–2318.

[26] Junkins, J. L., Akella, M. R., and Robinett, R. D. "Nonlinear adaptive control of spacecraft maneuvers". *AIAA*, 1997, pp. 1–9.

[27] Pan, H. and Kapila, V. "Adaptive nonlinear control for spacecraft formation flying with coupled translational and attitude dynamics". *40th IEEE Conference on Decisision and Control*, December, 2001, pp. 2057–2062.

[28] Kang, J.-Y. "Slosh Dynamics of Internal Mass in a Spinning Vehicle". *AIAA/AAS Astrodynamics Specialist Conference and Exhibit*, August, 2004, pp. 1–11.

[29] Ostroff, A. J. and Bacon, B. J. "Force and Moment Approach for Achievable Dynamics using Nonlinear Dynamic Inversion". *AIAA*, 1999, pp. 1–12.

[30] Janssens, F. L. and Ha, J. C. van der. "Stability of Spinning Satellite Under Axial Thrust, Internal Mass Motion, and Damping". *Journal of Guidance, Control, and Dynamics* 38.4, April, 2014, pp. 761–771.

[31] Atkins, B. and Queen, E. M. "Internal moving mass actuator based angle of attack and angle of sideslip control for Mars entry missions". *Advances in the Astronautical Sciences* 52.5, 2015, pp. 1294–1310.

[32] Juliana, S., Chu, Q. P., Mulder, J. A., and Baten, T. J. v. "Non-linear Dynamic Inversion versus Gain Scheduling Techniques for Re-entry Flight Control System". *56th International Astronautical Congress of the International Astronautical Federation, the International Academy of Astronautics, and the International Institute of Space Law*, 2005.

[33] Rogers, J. and Costello, M. "A Variable Stability Projectile Using an Internal Moving Mass". *AIAA Atmospheric Flight Mechanics Conference and Exhibit* August, August, 2008.